

November 29, 2002

# **Solvation Effects and Driving Forces for Protein Thermodynamic And Kinetic Cooperativity: How Adequate Is Native-Centric Topological Modeling?**

**Hüseyin KAYA and Hue Sun CHAN<sup>†</sup>**

Protein Engineering Network of Centres of Excellence (PENCE),  
Department of Biochemistry, and Department of Medical Genetics & Microbiology,  
Faculty of Medicine, University of Toronto, Toronto, Ontario M5S 1A8, Canada

**Running title:** Continuum Gō Model Chevron Plots

**Key words:** calorimetric cooperativity / single-exponential kinetics / unfolding / chevron plot / desolvation barrier / continuum Gō models / heat capacity

<sup>†</sup> Corresponding author.

E-mail address of Hue Sun CHAN: [chan@arrhenius.med.toronto.edu](mailto:chan@arrhenius.med.toronto.edu)

Tel: (416)978-2697; Fax: (416)978-8548

Mailing address: Department of Biochemistry, University of Toronto, Medical Sciences Building – 5th Fl., 1 King's College Circle, Toronto, Ontario M5S 1A8, Canada.

## Summary

What energetic and solvation effects underlie the remarkable two-state thermodynamics and folding/unfolding kinetics of small single-domain proteins? To address this question, we investigate the folding and unfolding of a hierarchy of continuum Langevin dynamics models of chymotrypsin inhibitor 2. We find that residue-based additive Gō-like contact energies, although native-centric, are by themselves insufficient for proteinlike calorimetric two-state cooperativity. Further native biases by local conformational preferences are necessary for proteinlike thermodynamics. Kinetically, however, even models with both contact and local native-centric energies do not produce simple two-state chevron plots. Thus a model protein’s thermodynamic cooperativity is not sufficient for simple two-state kinetics. The models tested appear to have increasing internal friction with increasing native stability, leading to chevron rollovers that typify kinetics that are commonly referred to as non-two-state. The free energy profiles of these models are found to be sensitive to the choice of native contacts and the presumed spatial ranges of the contact interactions. Motivated by explicit-water considerations, we explore recent treatments of solvent granularity that incorporate desolvation free energy barriers into effective implicit-solvent intraprotein interactions. This additional feature reduces both folding and unfolding rates vis-à-vis that of the corresponding models without desolvation barriers, but the kinetics remain non-two-state. Taken together, our observations suggest that interaction mechanisms more intricate than simple Gō-like constructs and pairwise additive solvation-like contributions are needed to rationalize some of the most basic generic protein properties. Therefore, as experimental constraints on protein chain models, requiring a consistent account of proteinlike thermodynamic and kinetic cooperativity can be more stringent and productive for some applications than simply requiring a model heteropolymer to fold to a target structure.

## INTRODUCTION

A fundamental unresolved question in molecular biology is how solvent-mediated interactions conspire to produce the highly specific structures and dynamics of proteins. Recent experiments on highly cooperative “two-state” folding/unfolding kinetics of small single-domain proteins<sup>1–4</sup> have, however, revealed an intriguing phenomenological simplicity. Most notably, the folding rates of these proteins are found to be well correlated with a simple contact order parameter deducible entirely from the native contact pattern, often referred to as a protein’s “topology.”<sup>1,5–7</sup>

From a reductionist viewpoint, protein behavior is ultimately determined by the large collection of atoms of the protein and those that constitute the solvent. Indeed, computational studies of protein folding by all-atom simulations have led to many useful insights.<sup>8–10</sup> As well, recent developments in Monte Carlo conformational sampling techniques are promising (see, e.g., ref. 10). However, currently even the most extensive all-atom explicit-solvent simulations of proteins<sup>8,9</sup> do not appear to provide sufficient conformational coverage to tackle many equilibrium and long-timescale kinetic properties under ambient conditions. Thus, a long-standing<sup>11–13</sup> complementary approach is to adopt simplified lattice<sup>14–19</sup> or continuum<sup>19–21</sup> representations of polypeptide geometries and interactions, trading high structural resolution for the extensive conformational sampling that is often necessary for conceptual advances.<sup>15–21</sup>

Considerable progress has been made using simplified representations. But still it has been exceedingly difficult to fold a heteropolymer chain to the native structure of a real protein by a potential function determined solely by the chain’s one-dimensional amino acid sequence. In this context, the recent discovery of certain predictive powers of native topology<sup>5</sup> has inspired intense interests in native-centric modeling.<sup>22–46</sup> These models are often called Gō or Gō-like since they make no explicit reference to a protein’s sequence. Instead, teleological<sup>47,48</sup> interaction schemes are postulated to bias conformations toward a given native structure, in a manner similar to the original lattice constructs of Gō and coworkers.<sup>12,49</sup>

Remarkably, despite their apparent simplicity and artificiality, tremendous advance

has been made by recent innovations in native-centric modeling. This investigative approach has proven to be a very effective tool to gain understanding in the face of difficulties encountered by more reductionist approaches.<sup>50</sup> Through the questions they posed, critical physical insights have been gained into the thermodynamics,<sup>27,28,30,32,37–41,45</sup> folding kinetics,<sup>30–35,38–46</sup> folding rates,<sup>22–25,35,43</sup> and transition states and folding intermediates<sup>26,31,32,36,40,42,43,46</sup> of proteins. For example, physical rationalizations of the observed relationship between contact order and folding rate have been provided by Ising-type native-centric models without an explicit chain representation<sup>23–25</sup> as well as explicit Gō-like chain models.<sup>35</sup> In separate efforts, using a protein’s database native structure as starting point, Gaussian elastic network<sup>51,52</sup> and graph theoretic<sup>53</sup> models have been notably successful in deciphering the flexibility and vibrational modes of real proteins without explicitly considering the myriad intraprotein interactions involved. These models of near-native dynamics do not originally tackle protein folding/unfolding kinetics. But in a recent generalization of the Gaussian elastic network model that took into account chain connectivity, a significant correlation between experimental folding rates and the relaxation rates of the slowest vibrational modes was discovered,<sup>44</sup> suggesting an intimate connection between near-native vibrations and folding/unfolding kinetics.

Some of the successes of native-centric approaches have been attributed to the stipulation<sup>28,32</sup> that Gō-like potentials are proteinlike to a certain degree because they serve to eliminate “to first order”<sup>28</sup> or to minimize<sup>32</sup> the “energetic frustration” that is presumed to be minimized in real proteins.<sup>54–56</sup> According to this view, native-centric models are thus left free to account for “topological frustration”<sup>28,32</sup> alone — i.e., to capture the physics arising solely from chain connectivity, excluded volume, and the favorability of the native fold.

While we cherish the successes of the native-centric paradigm, it is also important to not lose sight of its limitations. In short, native-centric modeling entails: (i) Admitting our ignorance of the basic physics of protein folding, at least for the time being. (ii) Recognizing that a protein sequence’s known native structure may contain significant information about its actual energetics. (iii) Assuming that a Gō-like potential inferred from the known native structure is in some sense an approximate description of the underlying physical energetics. (iv) Working out the logical consequences of these

assumptions to gain insight into various aspects of the folding process. In this perspective, native-centric modeling should be taken as a tentative means to capture collective atomic/molecular effects that we don’t yet understand. As such, its application may be physically more meaningful at a coarse-grained level (perhaps as a “renormalized” description). Although all-atom Gō-like models<sup>36,46</sup> are obviously superior in accounting for the important effects of sidechain packing (see, e.g., insightful discussion in ref. 46), physically it is even harder to justify why the interaction between a pair of atoms in general would depend on whether they are in close spatial proximity in a particular protein’s native structure. Historically speaking, the renewed popularity of Gō-like models in protein folding studies since the late 1990s may arguably represent a partial backtracking — albeit a very productive and well justified one — in modeling philosophy. This is so because the desire to supersede these earlier ad hoc interaction schemes appeared to be an impetus for the emergence since the late 1980s of simplified lattice protein folding models with general sequence-dependent potentials.<sup>57–62</sup>

Here we endeavor to better delineate the utility and limitation of several common native-centric approaches to protein folding. In identifying their strengths as well as weaknesses, our goal is to pave the way for improved native-centric modeling and better reductionist approaches. It goes without saying that Gō-like models are intrinsically incomplete, because (i) possible nonnative interactions are in large measure neglected,<sup>63,64</sup> and (ii) interaction (energetic) heterogeneities can be present in proteins with essentially identical topologies.<sup>65</sup> Practically speaking, even if a general usefulness of native-centric modeling is presumed, robustness of the predictions has to be ascertained. Many native-centric interaction schemes can be postulated; not all of them have the same predictions. Some discrepancies are puzzling. For example, the combination of a Gō-like potential with an explicit chain representation should, in principle, be a more adequate model of topological frustration<sup>28,32</sup> than models without an explicit chain representation. Yet so far native-centric constructs with geometrically less realistic (non-explicit) chain representations<sup>23–25,43</sup> appear to be more successful in reproducing experimental folding rates than direct folding kinetics simulations of Gō-like models with explicit chain representations.<sup>35</sup>

Specifically, the present work addresses two basic questions of robustness in native-

centric modeling: (i) How much do the model predictions depend on the choice of native contacts for a given protein? (ii) To what extent would these predictions be modified when the effects of the protein’s aqueous solvent are taken into account with more sophistication?<sup>40,66</sup> Pursuing a line of inquiry we have recently developed in the context of lattice models,<sup>18,47,48,67,68</sup> we focus here on whether continuum coarse-grained Gō-like energetics with an explicit chain representation can reproduce certain generic thermodynamic and kinetic cooperativities that have been experimentally observed across many real proteins. These statistical mechanics tests are stringent. For instance, the mere existence of a qualitatively sharp folding transition in a chain model does not necessarily imply that its underlying thermodynamics is proteinlike.<sup>18,47,48,67</sup> Homopolymers can have very sharp coil-globule transitions that are not calorimetrically two-state.<sup>69</sup> Comparisons between simulated and experimental chevron plots<sup>70</sup> show that even for chain models that satisfy the experimental thermodynamic two-state criteria, it is nontrivial<sup>68</sup> to reproduce the highly cooperative nonglassy two-state folding kinetics<sup>71</sup> of many small single-domain proteins. Therefore, applying these tests would, in due course, facilitate the improvement of existing models, suggest yet unexplored avenues of native-centric topological modeling, and ultimately help decipher the energetics of real proteins.

## COMPARING DIFFERENT NATIVE CONTACT SETS FOR CI2

We consider the 64-residue truncated form of chymotrypsin inhibitor 2 (CI2)<sup>72</sup> using coarse-grained  $C_\alpha$  representations with sidechain interactions accounted for by contacts between pairs of  $C_\alpha$  positions separated by at least three  $C_\alpha$ s along the chain sequence (contact order  $\geq 4$ ). CI2 is a widely studied small single-domain protein with no disulfide bond. It folds and unfolds as an apparent simple two-state system. CI2 is an ideal test case because a large body of experimental, all-atom molecular dynamics, and native-centric modeling data is available (see, e.g., refs. 32, 36, 73, 74). To investigate how coarse-grained native-centric model predictions may be sensitive to the definition of native contacts, here we examine two native contact sets, which we refer to as NCS1 and NCS2.

NCS1 is determined by the distance criterion of Shea et al.<sup>28</sup> Two amino acid residues

$i$  and  $j$  of a given protein are in contact if, in its native structure from the Protein Data Bank (PDB), either their  $C_\alpha$  atoms are less than 8 Å apart, or any two heavy atoms one from each of their two sidechains are less than 4 Å apart, or both. Using this definition, there are 137 NCS1 contacts. NCS2 is borrowed from Clementi et al.’s native contact map for CI2 (Figure 2 of ref. 32). NCS2 has 142 contacts. It was based upon the CSU software<sup>75</sup> which takes into account more detailed structural information\* such as contact surface area and solvent accessibility. There are considerable variations in native  $C_\alpha$ - $C_\alpha$  distances among contacts in both NCS1 and NCS2. The minimum native contact distance is 4.325 Å for both sets, but the maximum are 12.255 Å and 15.558 Å for NCS1 and NCS2 respectively. The average native distance of NCS1 (6.528 Å) is smaller than that of NCS2 (7.288 Å). However, the average sequence separations of NCS1 (23.1) and NCS2 (22.6) are almost identical.

Figure 1 compares the two native contact sets. They have 108 contacts in common (blue lines in Figure 1b). Among the native contacts that are not common to both sets, those belonging to NCS1 but not NCS2 (green lines in Figure 1c) tend to be between two ends of the chain or involve the  $\beta$ 1 strand (residues 27–34).<sup>73</sup> In contrast, contacts belonging to NCS2 but not NCS1 (red lines in Figure 1d) appear to be more uniformly distributed, involving more the  $\alpha$ -helix (residues 13–23) and the region spanning residues 35–44. Specific examples of these differences are provided in Figure 2, showing that NCS1 identifies an hydrophobic-polar (alanine-arginine) contact but not an hydrophobic-hydrophobic (valine-phenylalanine) contact.

## MODELS AND METHODS

### *Coarse-grained Potentials Without Solvation/Desolvation Barriers*

The basic construct of our native-centric potentials follows that of Clementi et al.<sup>32</sup> For a given model protein conformation specified by the positions of all its  $C_\alpha$  atoms,

---

\*For CI2, the current version of the CSU software available from the Internet also produces a set of 142 native contacts, all except 8 of which are identical to the contacts in NCS2. For the computational tests we have conducted (detailed data not shown), differences in results for this particular CSU native contact set and that for NCS2 are negligible.

the total Gō-like potential energy

$$\begin{aligned}
V_{\text{total}} &= V_{\text{stretching}} + V_{\text{bending}} + V_{\text{torsion}} + V_{\text{non-bonded}} \\
&= \sum_{\text{bonds}}^{N-1} K_r (r - r_0)^2 + \sum_{\text{angles}}^{N-2} K_\theta (\theta - \theta_0)^2 \\
&\quad + \sum_{\text{dihedrals}}^{N-3} \left\{ K_\phi^{(1)} [1 + \cos(\phi - \phi_0)] + K_\phi^{(3)} [1 + \cos 3(\phi - \phi_0)] \right\} \\
&\quad + \sum_{i < j-3}^{\text{native}} \epsilon \left[ 5 \left( \frac{r'_{ij}}{r_{ij}} \right)^{12} - 6 \left( \frac{r'_{ij}}{r_{ij}} \right)^{10} \right] + \sum_{i < j-3}^{\text{non-native}} \epsilon \left( \frac{r_{\text{rep}}}{r_{ij}} \right)^{12}, \tag{0.1}
\end{aligned}$$

where  $N$  is the total number of particles. This functional form has also been used by Koga and Takada.<sup>35</sup> Here the first three summations are for local interactions, where  $r$ ,  $\theta$ , and  $\phi$  are, respectively, the  $\text{C}_\alpha$ – $\text{C}_\alpha$  virtual bond length between successive residues along the chain sequence,  $\text{C}_\alpha$ – $\text{C}_\alpha$  virtual bond angles, and  $\text{C}_\alpha$ – $\text{C}_\alpha$  virtual torsion angles;  $r_0$ ,  $\theta_0$ , and  $\phi_0$  are the corresponding native values in the PDB structure. These terms account for chain connectivity and presumed local conformational preferences for the native fold. The last two summations are for nonlocal interactions;  $r_{ij}$  is the spatial distance between two  $\text{C}_\alpha$ s that have at least three residues between them along the chain sequence. In the summation over native contacts (as defined above for either NCS1 or NCS2), a 10–12 Lennard Jones (LJ) form is used, where  $r'_{ij}$  is the  $\text{C}_\alpha$ – $\text{C}_\alpha$  distance between the contacting residue  $i$  and residue  $j$  in the PDB structure. In the summation over non-native contacts,  $r_{\text{rep}}$  parametrizes the excluded volume repulsion between residue pairs that do not belong to the given native contact set. As in refs. 32 and 35, we use  $r_{\text{rep}} = 4 \text{ \AA}$  (whereas ref. 28 uses  $r_{\text{rep}} = 7.8 \text{ \AA}$ ). The ratios between interaction parameters are  $K_r = 100\epsilon$ ,  $K_\theta = 20\epsilon$ ,  $K_\phi^{(1)} = \epsilon$ , and  $K_\phi^{(3)} = 0.5\epsilon$ , as in ref. 32. The interaction strength is thus controlled by a single parameter  $\epsilon$ . We refer to the potential just described as the “without-solvation” model because it does not have a solvation/desolvation barrier (see below), although the terms in equation 1 may be interpreted as part of an implicit-solvent scheme that takes into account other aspects of solvent-mediated interactions.

Equation 1 assumes that native-centric favorable interactions have relatively long spatial ranges. In alternate square-well Gō models,<sup>41</sup> however, favorable contact interactions have sharp cutoffs. Moreover, in many lattice models, contact interactions may be viewed as having infinitesimal spatial ranges. Thus, to investigate how the presumed spatial ranges of contact interactions may affect model predictions, we study a variation



of the above model that restricts each of the pairwise 10–12 LJ native contact terms in equation 1 to  $r_{ij} \leq 1.2r'_{ij}$  and sets the interaction to zero for  $r_{ij} > 1.2r'_{ij}$ , but all other aspects of the model stay the same. We call this the “without-solvation-SSR” (short spatial range) model.

### *An Approximate Account of Solvation/Desolvation Barriers*

We consider also coarse-grained “with-solvation” models designed to semi-quantitatively account for the solvation/desolvation free energy barriers encountered by a protein’s constituent groups as they cluster together in aqueous solvents (Figure 3). We refer to these barriers simply as “desolvation barriers” below. Desolvation barriers are a robust consequence of granularity or the particulate nature of the solvent.<sup>76</sup> They have long been predicted by theory<sup>77</sup> and atomic simulations.<sup>78,79</sup> However, aside from an earlier study that used a square-well/square-shoulder form of desolvation barriers,<sup>66</sup> until very recently<sup>40,80,81</sup> this salient physical feature was not taken into account in continuum coarse-grained protein models. While explicit-solvent molecular dynamics account for solvation effects directly, these simulations do not yet provide a definitive answer as to whether they can or cannot reproduce the experimentally observed thermodynamic and kinetic cooperativities in protein folding. Therefore, complementary “implicit-solvent”<sup>82</sup> treatments<sup>40,66,79,80</sup> like the present approach are needed. Indeed, the experimentally based cooperative tests conducted here should also be applied to all-atom models once their computational efficiency has improved to make it possible.

The scope of the present work is limited. In particular, the study of structural details — such as connections to the powerful experimental  $\Phi$ -value analysis of transition-state structures,<sup>4,72,74</sup> is deferred to future applications of our investigative framework. We first tackle a little-explored but fundamental question: How deeply are protein folding thermodynamic and kinetic cooperativities affected by the introduction of generic desolvation barriers? To this end, we employ the general implicit-solvent functional form introduced recently by Cheung et al.<sup>40</sup> (Figure 3). The repulsive part of this potential (for  $r < r'$ ) is similar, though not identical, to the repulsive part of the 10–12 LJ term in the without-solvation model above (equation 1). The key difference is that now a free energy barrier is present at the midpoint  $(r' + r'')/2$  between the contact ( $r'$ ) and water-separated ( $r''$ ) free energy minima of a given pairwise interaction;  $r'' - r' = 3.0 \text{ \AA}$  is the approximate

diameter of a single water molecule. Shown in Figure 3b(i) is a potential with relative magnitudes of the barrier and minima similar to that in ref. 40. This form has a relatively high desolvation barrier.<sup>†</sup> The  $U(r)$  function in the present study has a lower barrier (Figure 3a). As our goal is only to elucidate the generic implications of having a significant desolvation barrier, provided that the barrier is not negligible, a lower barrier is advantageous because it allows for faster kinetics and thus broader conformational sampling. Not the least, our choice is not inconsistent with recent explicit-water atomic simulations that predicted a lower pairwise desolvation barrier<sup>83</sup> [Figure 3b(ii)]. Now, for the with-solvation model, we simply replace the pairwise 10–12 LJ terms of the second last summation over native contacts in the  $V_{\text{total}}$  equation 1 above with  $U(r)$ s (Figure 3a) for the corresponding native pairs. Other terms in equation 1 remain the same. We call the resulting potential function  $V_{\text{total}}^{(S)}$ . Again, the interaction strength of a given model is controlled by one single parameter  $\epsilon$ . In principle, terms in both the without-solvation and with-solvation potentials representing solvent-mediated interactions can depend on temperature.<sup>84–86</sup> To simplify the formulation, however, and especially since most of the results in this report entail comparing kinetic trajectories under a constant given temperature, here  $V_{\text{total}}$  and  $U(r)$  are taken to be temperature independent, as in refs. 32 and 40.

### *Langevin Dynamics*

Folding and unfolding kinetics are simulated by Langevin dynamics,<sup>‡</sup> using a formulation similar to Thirumalai and coworkers'.<sup>88,89</sup> For each of the  $3N$  degrees of freedom of the model protein ( $x$ ,  $y$  or  $z$  coordinates of the  $C_\alpha$ s), the equation of motion is:

$$m\dot{v}(t) = F_{\text{conf}}(t) - m\gamma v(t) + \eta(t) , \quad (0.2)$$

where  $m$ ,  $v$ ,  $\dot{v}$ ,  $F_{\text{conf}}$ ,  $\gamma$  and  $\eta$  are, respectively, mass, velocity, acceleration, conformational force, friction (viscosity) constant and random force. The conformational force is equal to the negative gradient of the total potential energy of the given model ( $V_{\text{total}}$  or  $V_{\text{total}}^{(S)}$ ). For the without-solvation-SSR models, conformational force from the pairwise 10–12 LJ native contact term in  $V_{\text{total}}$  between residues  $i$  and  $j$  is applied only if  $r_{ij} \leq 1.2r'_{ij}$ . The

---

<sup>†</sup>In order not to have a negative  $\epsilon''/\epsilon$  ratio, it appears that the relation  $(\epsilon'' - \epsilon')/(\epsilon' - \epsilon) = 1.33$  in the legend for Figure 1 in Cheung et al.<sup>40</sup> should read  $(\epsilon'' + \epsilon')/(\epsilon' - \epsilon) = 1.33$ .

<sup>‡</sup>Alternately, Newtonian dynamics in conjunction with the Berendsen et al. algorithm<sup>87</sup> for coupling to a heat bath was used by several previous investigations<sup>32,35</sup> of similar Gō-like coarse-grained protein models.

random force has the autocorrelation function

$$\langle \eta(t)\eta(t') \rangle = 2m\gamma k_B T \delta(t - t') , \quad (0.3)$$

where  $k_B T$  is Boltzmann constant times absolute temperature. Every  $C_\alpha$  is subject to a random force at each integration time step. The components of the random force are independently generated by setting  $\eta_i = (2m\gamma k_B T / \delta t)^{1/2} \xi_i$ . Here  $i$  denotes the uncorrelated random force components in the  $x$ ,  $y$  or  $z$  directions,  $\xi_i$  is a random value taken from a Gaussian distribution with zero mean and unit variance (obtained from a random number generator by standard techniques<sup>90</sup>), and  $\delta t$  is the integration time step. At the commencement of a simulation at temperature  $T$ , the initial velocities are assigned random values by setting  $v_i = (k_B T / m)^{1/2} \xi_i$ .

We use the velocity-verlet algorithm<sup>88–91</sup> (equations 12 and 13 in ref. 89) to integrate equation 2. Independent of simulation conditions such as variations in  $\epsilon$  and  $T$ , the time scale of the model systems here is always controlled by the quantity  $\tau = \sqrt{ma^2/\epsilon_0}$ , with the length scale  $a = 4 \text{ \AA}$  and a reference energy scale  $\epsilon_0 = 1$ . We further set  $\gamma = 0.05\tau^{-1}$  and use a molecular dynamics time step  $\delta t = 0.005\tau$  in the numerical integration. Conformational sampling is performed by averaging over snapshots taken at every 400 time steps. Simulation times in this study are presented in units of  $\delta t$ . The energy parameter  $\epsilon$  and temperature  $T$  are given respectively in units of  $\epsilon_0$  and  $\epsilon_0/k_B$ , and length is measured in units of  $\text{\AA}$ . To simplify notation, other units are chosen such that  $m = 1$  and  $k_B = 1$  in the present simulations, as in Veitshans et al.<sup>89</sup> An approximate correspondence between model time and real protein kinetic time scales can be found in ref. 89.

## THERMODYNAMIC COOPERATIVITY

### *Free Energy Profiles in Different Native-Centric Schemes*

Using the progress variable  $Q$  (native contact fraction), Figure 4 shows that conformational distribution is significantly sensitive to the choice of native contact set and the presumed spatial ranges of native contact interactions. Consistent with the expectation for a two-state protein such as CI2 and a previous without-solvation study,<sup>32</sup> the free energy profiles for NCS2 (solid curves) exhibit a single peak at intermediate  $Q$  separating the native (high  $Q$ ) and denatured (low  $Q$ ) minima. In contrast, the NCS1 free energy profile has a plateau-like transition region in the without-solvation formulation

(Figure 4a, dashed curve). More remarkably, for the without-solvation-SSR and with-solvation models (Figure 4b, c), the NCS1 profiles develop a shallow minimum flanked by two peaks in the intermediate  $Q$  region (dashed curves), similar to certain postulated free energy profiles discussed previously, for example, by Fersht<sup>92</sup> and Chu and Bai,<sup>93</sup> in the context of folding kinetics that apparently involves intermediates. Also notable is the progressive movement of the native minimum position from  $Q \approx 0.9$  for the without-solvation models toward  $Q = 1$  for the with-solvation models. The incorporation of desolvation barriers dramatically raises the overall folding/unfolding free energy barrier for NCS2, but only has a relatively subdued effect for NCS1 (c.f. Figure 4b, c), suggesting that there is an intricate interplay between desolvation barrier effects and other aspects of solvent-mediated interactions in protein folding.

### *Calorimetric Cooperativity: Local Conformational Preferences are Crucial*

Figure 5 assesses the calorimetric cooperativity<sup>47,48,67,68</sup> of seven different native-centric models of CI2 by comparing their simulated van’t Hoff over calorimetric enthalpy ratios  $\Delta H_{\text{vH}}/\Delta H_{\text{cal}}$  to the experimental two-state requirement that  $\Delta H_{\text{vH}}/\Delta H_{\text{cal}} \approx 1$ . Model intraprotein interactions are taken to be temperature independent in this evaluation. Since vibrations along the bonds (equation 1) contribute to heat capacity in these models outside the folding/unfolding transition region, and there is experimental evidence for heat capacity contributions from bond vector motion in real proteins,<sup>94</sup> the simulated  $\Delta H_{\text{vH}}/\Delta H_{\text{cal}}$  ratio without baseline subtractions does not correspond physically to the experimental  $\Delta H_{\text{vH}}/\Delta H_{\text{cal}}$  ratio obtained by empirical baseline subtractions.<sup>47,48,67,68</sup> Thus, only the baseline-subtracted  $\Delta H_{\text{vH}}/\Delta H_{\text{cal}}$  ratio  $\kappa_2^{(\text{s})}$  from the models are judged against the experimental calorimetric two-state criterion.<sup>47,48,68</sup> Figure 5 shows that  $\Delta H_{\text{vH}}/\Delta H_{\text{cal}} = \kappa_2^{(\text{s})} \approx 1$  is satisfied by all six models described in the last section. Apparently, similar Gō-like models in refs. 32 and 40 also exhibit calorimetric cooperativity. This is evident from their reported heat capacity scans although  $\Delta H_{\text{vH}}/\Delta H_{\text{cal}}$  ratios were not computed in these works.

The role of local interactions is addressed by a different coarse-grained model with Gō-like (through-space) contact interactions but very little local (through-bond) preference for the CI2 native structure. The setup of this “contact-dominant” model is similar

to that of the NCS2 without-solvation-SSR model: It has the same virtual bond strength ( $K_r = 100\epsilon$ ), but the local native preference is weakened by a factor of 20, i.e.,  $K_\theta = 0.5\epsilon$ ,  $K_\phi^{(1)} = 0.05\epsilon$ , and  $K_\phi^{(2)} = 0.025\epsilon$ . Folding in this model is clearly non-two-state. In our simulation of this contact-dominant model, conformations very close to the target native structure were observed but  $Q = 1$  was not achieved.<sup>§</sup> A numerical estimate of this model’s heat capacity function was obtained from Langevin dynamics simulation near the transition midpoint. Figure 5 shows that it has a double hump, which is clearly dissimilar to the single-peak heat capacity scans of two-state proteins such as CI2.<sup>72,95</sup> Moreover, near this model’s temperature for the peak heat capacity value, the distribution of  $Q$  has only a single population maximum rather than being bimodal (data not shown). Indeed, a few highest and lowest  $Q$  values were so improbable that they were not sampled. These thermodynamically non-cooperative features are reflected by an exceedingly low van’t Hoff over calorimetric enthalpy ratio of  $\kappa_2^{(s)} = 0.33$ .

One may conceivably argue from the “energetic vs. topological frustration” perspective<sup>28,32</sup> that energetic frustration has already been eliminated in the contact-dominant model because its potential favors native contacts, disfavors nonnative contacts, and even slightly favors native bond angles and torsion angles. Yet the contact-dominant model’s thermodynamics is not proteinlike. The non-cooperative behavior of this particular contact-dominant model might have been exasperated by the exclusion of  $(i, i + 3)$  contacts in its formulation (see equation 1). Nonetheless, the present result echoes several recent findings of less-than-proteinlike thermodynamic cooperativity in continuum models with Gō-like contact interactions but without local conformational preferences. These model studies include coarse-grained and all-atom discontinuous molecular dynamics models<sup>41,45</sup> as well as a self-consistent field theory.<sup>37</sup> On the other hand, some three-dimensional lattice “contact-only” Gō models are thermodynamically cooperative,<sup>47</sup> probably because of default lattice restrictions on bond angles and torsion angles. However, in continuous space, the “negative design” afforded by Gō-like contact interactions alone are apparently insufficient for proteinlike thermodynamics. Indeed, a protein sequence’s ability to fold to a unique structure may be partially encoded in local signals.<sup>96,97</sup> Proteinlike

---

<sup>§</sup>We have also studied similar “contact-only” models with  $K_\theta = K_\phi^{(1)} = K_\phi^{(2)} = 0$  in the same without-solvation-SSR setup as well as in the (full LJ) without-solvation formulation. These models have even bigger difficulties reaching conformations with  $Q \approx 1$  than the contact-dominant model.

behavior requires minimization of energetic frustration of the target native structure as well as enhanced frustration in the competing nonnative conformations.<sup>98</sup> A comparison between the contact-dominant model and the other models with local native propensities in Figure 5 suggests that an interplay between local conformational preference and nonlocal compactification forces<sup>47,48,67,68,99,100</sup> are necessary for proteinlike thermodynamic cooperativity. For this conclusion to be properly interpreted, we hasten to add that structural details of sidechain packing, hydrogen bonding, as well as general non-native-centric physical restrictions on bond angles and torsion angles (as in standard non-Gō-like force fields) have not been taken into account in the present coarse-grained (residue-based) contact-dominant model. But these effects are operative in real proteins. Clearly, these interactions must be part of the physical basis of any local propensity<sup>101</sup> for the native fold in a more complete all-atom description.

## KINETIC COOPERATIVITY

### *Sharp Kinetic Transitions Between Two Thermodynamic States*

Folding kinetics in explicit-chain Gō-like models have been investigated using equilibrium sampling in conjunction with free energy profile analyses<sup>32</sup> as well as direct dynamics simulations.<sup>35</sup> Here, around their respective transition midpoints, all six native-centric CI2 models — NCS1 or NCS2, with or without solvation — have kinetic characteristics consistent with their thermodynamic two-state cooperativity. Figure 6a and b show that the kinetic transitions between the native and denatured ensembles are sudden and sharp. Figure 6c and d show that the distributions of potential energy and  $Q$  are bimodally well separated into native and denatured regions, and the correlation between potential energy and  $Q$  is generally linear. A consistency check has also been made using Figure 6c, which provided an average kinetic energy of 78.9. Equating this with  $3NT/2$  for  $N = 64$  (equipartition theorem) yields  $T = 0.8219$ , which is essentially identical to the input simulation temperature of  $T = 0.82$ , as it should. Figure 6c and d further indicate that after the initiation of folding around the transition midpoint, pre-equilibration of the denatured ensemble is rapid relative to the folding time scale.

### *Chevron Plots: Matching Kinetics with Thermodynamics?*

Bearing in mind that protein thermodynamic cooperativity is necessary but not sufficient for simple two-state folding/unfolding kinetics,<sup>68</sup> we proceed to evaluate model predictions against experimental stability curves and chevron plots. To do so, we determine model folding and unfolding rates using direct dynamics simulations over extensive ranges of native stability by varying the interaction parameter  $\epsilon$  at constant temperature. Since the simulated kinetics are essentially single-exponential (see below), the folding or unfolding rate may be taken to be approximately the reciprocal of the corresponding mean first passage time (MFPT). The natural logarithms of the rates are plotted as functions of  $\epsilon$  in Figures 7 – 9. Inasmuch as it was computationally feasible, first passage times (FPTs) of a large number of trajectories were used to provide reliable estimates of MFPTs (Tables 1 – 3). As one of us has argued,<sup>98,102</sup> the variation of  $\epsilon$  may serve as a tentative model for varying denaturant concentration, though the detailed physics of how the effects of chemical denaturants should be incorporated into coarse-grained protein models is a subject of ongoing research.<sup>103–106</sup> Here we view the upper panels of Figures 7 – 9 as model equivalences of chevron plots.

Native stability curves of the models as functions of  $\epsilon$  are plotted in the lower panels of Figures 7 – 9. They show that the free energy of unfolding between the native minimum and low- $Q$  open conformations are approximately linear in  $\epsilon$  (upper solid and dashed curves). These quasi-linear stability curves estimated from simulation data around the transition midpoint correspond to those obtained experimentally by empirical linear extrapolation from directly measured data around the transition region.<sup>107</sup> In contrast, the free energy difference between the native minimum and a denatured-state ensemble encompassing low- $Q$  as well as intermediate- $Q$  conformations (lower solid and dashed curves) is nonlinear in  $\epsilon$ , similar to that observed in previously lattice model studies.<sup>67,68</sup> This is an expected feature<sup>67,68</sup> intimately connected to the multiple-conformation nature of the native state,<sup>47,68</sup> and is consistent with recent native-state hydrogen exchange experiments.<sup>107–110</sup> These characteristics of native stability underscore the fact that the operational definition of calorimetric two-state behavior (see above) does not<sup>67</sup> necessarily imply that all denatured conformations have the same stability. Even for calorimetrically two-state proteins under native conditions well below the global folding/unfolding transition midpoint, the population of partially unfolded conformations<sup>67,68,107,111</sup> can sometimes be non-negligible as long as it does not exceed a certain threshold.<sup>67,68</sup>

Figures 7 – 9 show that the transition midpoints determined by thermodynamics and kinetics are quite close, with only minor discrepancies. The discrepancies for NCS1 models appear to be slightly larger in Figures 8 and 9. This is probably related to the high-free-energy minima in the transition regions of the corresponding NCS1 free energy profiles (Figure 4b, c). More surprisingly, however, is that even with their native-centric potentials, all six models fail to produce the type of simple two-state folding/unfolding kinetics observed experimentally for CI2<sup>95</sup> and many other small single-domain proteins.<sup>7</sup> The operational definition<sup>95,112</sup> for simple two-state folding/unfolding kinetics requires that the logarithmic folding and unfolding rates under constant temperature be approximately linear in native stability, and that the natural logarithm of the directly measured and linearly extrapolated (folding rate)/(unfolding rate) ratio as a function of denaturant concentration matches the directly measured and linearly extrapolated<sup>95,107</sup> equilibrium free energy of unfolding in units of  $k_B T$ . Here, the dashed-dotted V-shapes in the upper panels of Figures 7 – 9 show that as  $-\epsilon/k_B T$  is changed at constant  $T$  from the transition midpoint towards either more native or more denaturing conditions, the respective trends of increase in simulated folding or unfolding rate fall short of this requirement for the kinetics to be simple two-state. Instead, our models’ behavior is more akin to proteins that exhibit chevron rollovers, such as ribonuclease A<sup>113</sup> and barnase,<sup>114</sup> whose kinetics are operationally referred to as non-two-state.<sup>68,95,113,114</sup> Comparisons with experimental chevron plots have not been made in other studies of continuum Gō models, but the reported results indicate that they also do not predict simple two-state chevron behavior (see, e.g., Figure 2 of ref. 34).

The four without-solvation and without-solvation-SSR models in Figures 7 and 8 show a clear rollover in both the folding and unfolding arms of their chevron plots. Reflecting the lower barriers along their free energy profiles (Figure 4), kinetics are generally faster for the without-solvation and without-solvation-SSR than the corresponding with-solvation models (Figure 9). For the with-solvation models, the rate at a given  $-\epsilon/k_B T$  is substantially slower for NCS2 than that for NCS1. This trend is consistent with NCS2’s much higher free energy barrier in the transition region (Figure 4c). Most remarkably, comparing Figures 7, 8 against Figure 9 demonstrates a dramatic impact of desolvation barriers on the folding/unfolding kinetics. In contrast to the chevron plots



with significant curvatures for the without-solvation and without-solvation-SSR models, both the folding and unfolding arms of the chevron plots are quasi-linear for the with-solvation models. It is reassuring that the with-solvation models are more proteinlike in this respect.<sup>113,114</sup> Nevertheless, their deviations from simple two-state kinetics are huge: The slopes of the simulated chevron plots are only approximately 1/5 that required for simple two-state kinetics (c.f. the V-shape in the upper panel of Figure 9). Therefore, the conclusion that these models' kinetics correspond to those operationally referred to as non-two-state should be reliable. This is because possible numerical uncertainties in the estimation of stability curves by histogram techniques (lower panels of Figure 9) are not likely to cause a factor-of-five discrepancy. Interestingly, similar mismatches between extrapolated chevron plots and direct native stability measurements, albeit to a lesser degree, have also been observed for real proteins.<sup>93</sup>

### *Single-Exponential Relaxation*

Experimentally, kinetic relaxation of many small single-domain proteins<sup>7</sup> such as CI2<sup>72,95</sup> and some apparently non-two-state proteins with chevron rollovers<sup>113,114</sup> are found to be essentially single-exponential. Therefore, it is of interest to ascertain whether the present models embody this hallmark, even though they are not kinetically simple two-state. For this purpose, we examine the distributions of first passage times (FPTs, as defined in Figures 7 – 9). Let  $P(t)dt$  be the probability for the FPT of a given kinetic process to lie within a range  $dt$  around time  $t$ . If the relaxation is single-exponential,

$$\int_{t_0}^t dt' P(t') = 1 - e^{-k(t-t_0)}, \quad (0.4)$$

where  $k$  is the kinetic rate, and  $t_0 \geq 0$  is a minimum FPT to take into consideration the finite time needed for pre-equilibration after initiation of the kinetic process at  $t = 0$ . It follows that

$$\text{MFPT} = \int_{t_0}^t dt' t' P(t') = t_0 + \frac{1}{k}. \quad (0.5)$$

To assess whether a given FPT distribution conforms to this description, a quantity  $P(t)\Delta t$  is computed by binning FPTs into time slots<sup>115</sup> of size  $\Delta t$ . If the kinetic process is single-exponential,

$$\ln[P(t)\Delta t] = \left\{ \ln\left(\frac{\Delta t}{\text{MFPT} - t_0}\right) + \frac{t_0}{\text{MFPT} - t_0} \right\} - \frac{t}{\text{MFPT} - t_0}, \quad (0.6)$$

i.e.,  $\ln[P(t)\Delta t]$  versus  $t$  should be a straight line with slope  $= -(\text{MFPT} - t_0)^{-1}$ .

Figure 10a shows that even under strongly native conditions concomitant with a significant chevron rollover, the NCS2 without-solvation-SSR model has approximately single-exponential relaxation. This behavior echoes that of a recent four-helix-bundle lattice model<sup>68</sup> (Figure 10b). Consistent with equation 6, a comparison between the filled and open circles in Figure 10a indicates that while changing the bin size  $\Delta t$  naturally changes the  $\ln[P(t)\Delta t]$  values, reasonable variations in  $\Delta t$  do not affect the slope of the  $\ln[P(t)\Delta t]$  distribution. Figure 11 applies similar analyses to folding and unfolding in other models in the present study under representative native and denaturing conditions.<sup>¶</sup> Owing to computational limitations, the sample sizes for the FPT distributions are not very large, especially for the with-solvation models in Figure 11c. Consequently, a certain level of statistical uncertainties ensued. Nonetheless, Figure 11 shows that for all cases tested, our data is consistent with single-exponential relaxation. As pointed out by Fersht,<sup>92</sup> the high-free-energy minima along the NCS1 free energy profiles (Figure 4b, c) do not preclude apparent single-exponential kinetics. The viability of equation 6 for our models is further buttressed by the relatively small differences between the slopes of the least-square-fitted lines in Figure 11 and the quantity  $-(\text{MFPT} - t_0)^{-1}$ , where  $t_0$  is taken to be the minimum FPT encountered in the simulated trajectories of a given model: For the models and their simulation conditions listed in the legend of Figure 11, and in the same order,  $\{[10^6 \times (\text{MFPT} - t_0)^{-1}], [-10^6 \times \text{slope}]\} = \{10.0, 10.6\}, \{6.13, 6.71\}, \{6.11, 6.53\}, \{7.28, 7.56\}, \{28.6, 36.1\}, \{6.41, 7.02\}, \{19.5, 26.4\}, \{8.53, 9.36\}, \{2.05, 2.08\}, \{0.504, 0.431\}, \{0.242, 0.189\}, \text{ and } \{0.199, 0.161\}.$

The native-centric formulations in the present Gō-like models lead to folding rates that are at least four orders of magnitude faster than the experimental CI2 folding rates. At 25°C and pH 6.3, the experimental CI2 folding rates at zero denaturant (native stability  $\Delta G = 12.0k_B T$ ) and the transition midpoint (in 3.92 M GdnHCl, native stability  $\Delta G = 0$ ) are, respectively,  $47.8 \text{ sec}^{-1}$  and  $0.035 \text{ sec}^{-1}$  (ref. 95). If we use the physical argument of Veitshans et al.<sup>89</sup> to identify the Langevin time unit  $\delta t$  with a real time scale of  $\sim 10^{-14} \text{ sec}$ , the folding rate of the NCS2 with-solvation model in Figure 9 is  $\sim 10^6 \text{ sec}^{-1}$  at  $\Delta G = 12.0k_B T$  and  $\sim 10^5 \text{ sec}^{-1}$  at  $\Delta G = 0$ . Corresponding folding

---

<sup>¶</sup>Rates in the chevron plots in Figures 7 – 9 are computed by taking  $t_0 = 0$ . Our calculations indicate that using finite  $t_0$ s instead of  $t_0 = 0$  to determine the rates  $k$  via equation 5 only leads to minimal modifications on the chevron plots (data not shown). The conclusions regarding rollovers and non-two-state kinetics remain unchanged.

rates of other models in Figures 7 – 9 are even faster by approximately two orders of magnitude. Despite these discrepancies, native-centric constructs do capture part of real protein energetics. This is evident from studies of extensive sets of real proteins using explicit-chain Gō models, wherein theoretically predicted folding<sup>35</sup> and relaxation<sup>44</sup> rates were found to correlate reasonably well with the experimental folding rates. However, it is noteworthy that the spread of these model-predicted rates among the set of proteins tested is apparently at least 1.5 – 2 orders of magnitude narrower than the diversity of experimental folding rates.<sup>35</sup> (c.f. Figure 5 of ref. 44). This suggests that certain basic aspects of protein energetics are yet to be taken into account by common Gō-like models. In a similar vein, the chevron rollovers in Figures 7 – 9 represent a failure to account for the high degree of diversity in folding rates of a given protein under different native conditions. For real CI2, the folding rates at zero denaturant and at the transition midpoint differ by three orders of magnitude. But the Gō-like models in Figures 7 – 9 predict only one order of magnitude difference.

### *Chevron Rollover: Stability-Dependent Front Factor?*

To better understand the chevron rollovers, Figure 12 applies a protocol we recently developed<sup>68</sup> to assess the models’ conformity to the commonly employed transition state picture in interpreting protein folding experiments. Model data is now fitted to the expression

$$\text{rate} = F(\epsilon, T) \exp \left[ -\frac{\Delta G^\ddagger(\epsilon, T)}{k_B T} \right] \quad (0.7)$$

for folding or unfolding rate, taken as (MFPT)<sup>−1</sup> from the direct dynamics simulations. On the other side of the above equation,  $\Delta G^\ddagger$  is an activation free energy determined solely by thermodynamic Boltzmann weights<sup>68</sup> using the method of Nymeyer et al.,<sup>32,116</sup>  $F$  is the corresponding front factor.<sup>2,38,39,68,98,117</sup> Figure 12 shows that, in contrast to the usual stipulation<sup>118</sup> that the front factors of small single-domain proteins such as CI2 are essentially independent of intraprotein interaction strength and native stability, the  $F$  factors deduced from the present analysis are highly sensitive to  $\epsilon$ . This implies that thermodynamic analyses of free energy profiles alone cannot predict the  $\epsilon$ -dependencies of the kinetic rates,<sup>38,39,68,117</sup> and the chevron rollovers are underpinned by native-stability-dependent front factors in these models.<sup>68</sup> This hypothesis regarding the physical origin of chevron rollover may soon be testable by single-molecule techniques.<sup>119</sup> In addition to the definitions for unfolded, transition, and folded regions in Figure 12, we analyzed

several other physically reasonable alternate  $Q$ -based definitions for these states (data not shown). Whereas the absolute value of  $F$  varies somewhat, the overall trend of dependence on  $\epsilon$  remains essentially unchanged. This resilience is similar to that observed in our previous analysis of the folding front factor of a 55mer lattice model (Figure 5 of ref. 68).

Thus, for this key aspect of chevron behavior, the present native-centric models' kinetics clearly do not resemble the simple two-state kinetics of CI2.<sup>72,95</sup> The ramifications of this finding is far reaching, as it bears on the basic energetics of protein folding (see Discussion below). As they stand, the apparently non-two-state kinetics of these physical self-contained polymer models<sup>18</sup> also shed light on the folding of other proteins that exhibit similar chevron rollovers as well.<sup>93,113,114</sup> To date, rationalizations of chevron rollovers include deadtime intermediates,<sup>120</sup> specific kinetic traps,<sup>98,102,121</sup> peak-shifting on complex free energy profiles,<sup>93,122</sup> burst phase continuum,<sup>123</sup> and internal friction as manifested by front factors that depend on native stability (ref. 68 and discussion therein). These perspectives are not necessarily mutually exclusive. For example, internal friction may arise from kinetic trapping mechanisms (H. K. & H. S. C., in preparation). In any event, chevron rollover is an unequivocal prediction of the present models, irrespective of whether  $Q$  or other folding reaction coordinates are used for the transition state analysis (see, e.g., ref. 124). Figure 12d shows that the folding front factor decreases with more native conditions, and the unfolding front factor also decreases with more denaturing conditions. In short, there appears to be an aversion to speed in these models' energetics. We tentatively attribute the slowing down in these models to a possible combination of effects of internal friction (conformational search problems compounded by more native conditions)<sup>68</sup> and external friction (implicit solvent viscosity). The origins of these effects remain to be better elucidated. For example, in some modeling situations,<sup>68</sup> folding-arm rollovers are related to the onset of downhill folding.<sup>125,126</sup> The chevron rollovers in the folding and unfolding arms of the NCS2 without-solvation model may be similarly related to downhill scenarios (see, e.g., the  $\epsilon = 0.90$  and  $\epsilon = 0.70$  profiles in Figure 12a). At least for the NCS2 with-solvation model in Figure 6, the fact that no deadtime intermediate was observed during our simulation suggests that such a mechanism is not necessary for chevron rollovers.<sup>68,93</sup> In this example, chevron rollover emerges as a kinetic front-factor effect.

## DISCUSSION

We have compared two different native contact sets, and three different formulations of Gō-like interactions with and without desolvation barriers. The predictions of these native-centric models were evaluated against generic thermodynamic and kinetic properties of small single-domain proteins that these models were designed to mimic in the first place. We learnt several lessons. First, proteinlike thermodynamic cooperativity requires nonlocal contact-like interactions acting in concert with local conformational favorabilities for the native fold<sup>47,48,67,68</sup> (Figure 5). Second, some basic predictions of native-centric models, such as the free energy profiles in Figure 4, are significantly dependent on the native contact set and interaction scheme used, even if the choice is made among physically reasonable definitions. A recent study<sup>38,39</sup> shows also that free energy profiles of native-centric models are sensitive to the chain’s presumed persistence length and energetic barriers to bond rotations.<sup>98,102</sup> Third, we found that pairwise desolvation barriers in native-centric models could lead to some proteinlike properties such as a higher free energy barrier separating the native and denatured states (c.f. Figure 4a, b and c) as well as more linear chevron plots (c.f. Figures 7, 8 and 9). These predictions are encouraging as they provide insight into corresponding features in real proteins. Fundamentally, however, the kinetics of all present native-centric models for CI2 do not resemble that of real CI2. The models with pairwise desolvation barriers, like those without, are kinetically non-two-state in the operational sense that they have large chevron rollovers.

Fourth, the significant differences between the predictions of with- and without-solvation models underscore the importance of proper accounting for the energetic cost of water expulsion in protein folding models, and that caution should be used when interpreting results obtained from effective potentials that do not have desolvation barriers.<sup>83,127</sup> The barrier height in the present with-solvation models simulated at  $T = 0.82$  is  $0.24 \epsilon k_B T$ . For real proteins, the desolvation barrier heights encountered by the polypeptide chain as a part of the potential of mean force are expected to be sensitive to temperature. Thus, the present results should also bear on explicit-solvent unfolding simulations at

high temperatures and the degree of dependencies of protein folding mechanisms on temperature.<sup>128</sup> Of relevance here is the model system of a pair of methanes in water. Recent Monte Carlo simulations in the TIP4P water model indicate that their desolvation barrier is reduced from approximately 0.16 to 0.12 kcal/mol ( $0.27k_{\text{B}}T$  to  $0.16k_{\text{B}}T$ ) when temperature is increased from 298K to 368K under atmospheric pressure.<sup>84</sup> Under typical high-temperature unfolding conditions of 498K and a water density of 0.829 gm/ml,<sup>128</sup> the desolvation barrier height is further reduced to  $\approx 0.05$  kcal/mol or  $0.05k_{\text{B}}T$  (Figure 16.3 in ref. 18; S. Shimizu and H. S. C., personal communication).

In a broader perspective, solvent-mediated interactions are known to be intrinsically pairwise nonadditive,<sup>76,83</sup> and the collapse of a hydrophobic chain may involve large length-scale dynamic effects.<sup>129</sup> In this light, that the pairwise desolvation barriers here fail to produce simple two-state chevron plots is not too surprising. Indeed, recent explicit-water simulations show that the sign of heat capacity of the free energy barrier against folding is opposite to that against the association of a pair of methane molecules.<sup>84,85,106</sup> Considerations of a three-methane model system further indicate that the height of desolvation barrier is clearly nonadditive, and the sign and magnitude of this nonadditivity is dependent upon the configuration of the nonpolar solutes involved.<sup>83</sup> Hence, solvation effects beyond the pairwise formulation considered here are likely needed to account for simple two-state protein folding/unfolding kinetics.

In summary, the present findings imply that the actual solvent-mediated interactions in real proteins are much more specific and well-designed than one would otherwise posit. In short, real proteins are more cooperative than common Gō-like models with pairwise additive interactions. Nonetheless, recent innovations in native-centric modeling have been immensely valuable. As discussed above, they do capture part of the essential physics. Many deep insight would not have been gained without them (see, e.g., refs. 1, 29, 33). But, at the same time, the limitations of common Gō-like chain models<sup>67,68</sup> may be more basic than previously appreciated. The present analysis implies that more proteinlike interaction schemes are yet to be discovered. Every model considered here except the contact-dominant variety can fold to the CI2 native structure. Qualitatively, the free energy profiles of the NCS2 models fit the expectation for that of small single-domain proteins as well. Yet their kinetics are fundamentally different from that of CI2. Thus, a

protein model’s ability to fold to one single target structure does not guarantee the adequacy of its energetics; and the microscopic origin of simple two-state folding/unfolding kinetics remains to be elucidated. Our effort to address some of these questions is underway. Apparently, chevron rollovers can be essentially eliminated in more cooperative chain models with added energetic favorabilities for the ground-state and near-ground-state structures beyond that provided by the additive schemes in common Gō models. These results will be presented in a subsequent report (H. K. & H. S. C., in preparation). In the ongoing quest for a better understanding of protein energetics through the design and interpretation of novel physical models, proteinlike statistical mechanics properties such as calorimetric two-state cooperativity<sup>41,47,48,67,68,130,131</sup> and simple two-state chevron behavior<sup>68</sup> should be useful as stringent but necessary modeling constraints.

## Acknowledgments

We thank Yawen Bai, Margaret Cheung, Cecilia Clementi, Ken Dill, Angel García, Chinlin Guo, Carol Hall, Anders Irbäck, Sophie Jackson, John Karanicolas, Bob Matthews, Cristian Micheletti, Hugh Nymeyer, Mikael Oliveberg, José Onuchic, Kevin Plaxco, John Portman, Eugene Shakhnovich, Joan-Emma Shea, Seishi Shimizu, Kim Sneppen, Dev Thirumalai, Michele Vendruscolo, Peter Wolynes, and Yaoqi Zhou for helpful discussions during the period in which these ideas were developed. This work was partially supported by the Canadian Institutes of Health Research (CIHR grant no. MOP-15323), a Premier’s Research Excellence Award from the Province of Ontario, and the Ontario Centre for Genomic Computing at the Hospital for Sick Children in Toronto. H. S. C. is a Canada Research Chair in Biochemistry.

## References

- [1] Baker, D. (2000). A surprising simplicity to protein folding. *Nature* **405**, 39–42.
- [2] Bilsel, O. & Matthews, C. R. (2000). Barriers in protein folding reactions. *Adv. Protein Chem.* **53**, 153–207.
- [3] Eaton, W. A., Muñoz, V., Hagen, S. J., Jas, G. S., Lapidus, L. J., Henry, E. R. & Hofrichter, J. (2000). Fast kinetics and mechanisms in protein folding. *Annu. Rev. Biophys. Biomolec. Struct.* **29**, 321–359.
- [4] Fersht, A. R. (2000). Transition-state structure as a unifying basis in protein-folding mechanisms: Contact order, chain topology, stability, and the extended nucleus mechanism. *Proc. Natl. Acad. Sci. USA* **97**, 1525–1529.
- [5] Plaxco, K. W., Simons, K. T. & Baker, D. (1998). Contact order, transition state placement and the refolding rates of single domain proteins. *J. Mol. Biol.* **277**, 985–994.
- [6] Chan, H. S. (1998). Matching speed and locality. *Nature* **392**, 761–763.
- [7] Plaxco, K. W., Simons, K. T., Ruczinski, I. & Baker, D. (2000). Topology, stability, sequence, and length: Defining the determinants of two-state protein folding kinetics. *Biochemistry* **39**, 11177–11183.
- [8] Duan, Y. & Kollman, P. A. (1998). Pathways to a protein folding intermediate observed in a 1-microsecond simulation in aqueous solution. *Science* **282**, 740–744.
- [9] Daggett V. (2002). Molecular dynamics simulations of the protein unfolding/folding reaction. *Acc. Chem. Res.* **35**, 422–429.
- [10] Sanbonmatsu, K. Y. & García, A. E. (2002). Structure of Met-enkephalin in explicit aqueous solution using replica exchange molecular dynamics. *Proteins Struct. Funct. Genet.* **46**, 225–234.
- [11] Levitt, M. & Warshel, A. (1975). Computer simulation of protein folding. *Nature* **253**, 694–698.



- [12] Taketomi, H., Ueda, Y. & Gō, N. (1975). Studies on protein folding, unfolding and fluctuations by computer simulation. 1. The effect of specific amino acid sequence represented by specific inter-unit interactions. *Int. J. Pept. Protein Res.* **7**, 445–459.
- [13] Hagler, A. T. & Honig, B. (1978). On the formation of protein tertiary structure on a computer. *Proc. Natl. Acad. Sci. USA* **75**, 554–558.
- [14] Godzik, A., Kolinski, A. & Skolnick, J. (1993). Lattice representations of globular proteins: How good are they? *J. Comp. Chem.* **14**, 1194–1202.
- [15] Bryngelson, J. D., Onuchic, J. N., Socci, N. D. & Wolynes, P. G. (1995). Funnels, pathways, and the energy landscape of protein folding: A synthesis. *Proteins Struct. Funct. Genet.* **21**, 167–195.
- [16] Dill, K. A., Bromberg, S., Yue, K., Fiebig, K. M., Yee, D. P., Thomas, P. D. & Chan, H. S. (1995). Principles of protein folding — A perspective from simple exact models. *Protein Sci.* **4**, 561–602.
- [17] Thirumalai, D. & Woodson S. A. (1996). Kinetics of folding of proteins and RNA. *Acc. Chem. Res.* **29**, 433–439.
- [18] Chan, H. S., Kaya, H. & Shimizu, S. (2002). Computational methods for protein folding: Scaling a hierarchy of complexities. In *Current Topics in Computational Molecular Biology*, eds. Jiang, T., Xu, Y. & Zhang, M. Q. (The MIT Press, Cambridge, MA), pp. 403–447.
- [19] Mirny, L. & Shakhnovich, E. (2001). Protein folding theory: From lattice to all-atom models. *Annu. Rev. Biophys. Biomol. Struct.* **30**, 361–396.
- [20] Thirumalai, D. & Klimov, D. K. (1999). Deciphering the timescales and mechanisms of protein folding using minimal off-lattice models. *Curr. Opin. Struct. Biol.* **9**, 197–207.
- [21] Onuchic, J. N., Nymeyer, H., García, A. E., Chahine, J. & Socci, N. D. (2000). The energy landscape theory of protein folding: Insights into folding mechanisms and scenarios. *Adv. Protein Chem.* **53**, 87–152.
- [22] Burton, R. E., Myers, J. K. & Oas, T. G. (1998). Protein folding dynamics: Quantitative comparison between theory and experiment. *Biochemistry*, **37**, 5337–5343.

- [23] Alm, E. & Baker, D. (1999). Prediction of protein-folding mechanisms from free-energy landscapes derived from native structures. *Proc. Natl. Acad. Sci. USA* **96**, 11305–11310.
- [24] Debe, D. A. & Goddard, W. A. (1999). First principles prediction of protein folding rates. *J. Mol. Biol.* **294**, 619–625.
- [25] Muñoz, V. & Eaton, W. A. (1999). A simple model for calculating the kinetics of protein folding from three-dimensional structures. *Proc. Natl. Acad. Sci. USA* **96**, 11311–11316.
- [26] Galzitskaya, O. V. & Finkelstein, A. V. (1999). A theoretical search for folding/unfolding nuclei in three-dimensional protein structures. *Proc. Natl. Acad. Sci. USA* **96**, 11299–11304.
- [27] Micheletti, C., Banavar, J. R., Maritan, A. & Seno, F. (1999). Protein structures and optimal folding from a geometrical variational principle. *Phys. Rev. Lett.* **82**, 3372–3375.
- [28] Shea, J.-E., Onuchic, J. N. & Brooks, C. L. III. (1999). Exploring the origins of topological frustration: Design of a minimally frustrated model of fragment B of protein A. *Proc. Natl. Acad. Sci. USA* **96**, 12512–12517.
- [29] Takada, S. (1999). *Gō*-ing for the prediction of protein folding mechanisms. *Proc. Natl. Acad. Sci. USA* **96**, 11698–11700.
- [30] Zhou, Y. & Karplus M. (1999). Interpreting the folding kinetics of helical proteins. *Nature* **401**, 400–403.
- [31] Clementi, C., Jennings, P. A. & Onuchic, J. N. (2000). How native-state topology affects the folding of dihydrofolate reductase and interleukin-1 $\beta$ . *Proc. Natl. Acad. Sci. USA* **97**, 5871–5876.
- [32] Clementi, C., Nymeyer, H. & Onuchic, J. N. (2000). Topological and energetic factors: What determines the structural details of the transition state ensemble and “en-route” intermediates for protein folding? An investigation for small globular proteins. *J. Mol. Biol.* **298**, 937–953.

- [33] Banavar, J. R. & Maritan, A. (2001). Computational approach to the protein-folding problem. *Proteins Struct. Funct. Genet.* **42**, 433–435.
- [34] Cieplak, M. & Hoang, T. X. (2001). Kinetic nonoptimality and vibrational stability of proteins. *Proteins Struct. Funct. Genet.* **44**, 20–25.
- [35] Koga, N. & Takada, S. (2001). Roles of native topology and chain-length scaling in protein folding: A simulation study with a Gō-like model. *J. Mol. Biol.* **313**, 171–180.
- [36] Li, L. & Shakhnovich, E. I. (2001). Constructing, verifying, and dissecting the folding transition state of chymotrypsin inhibitor 2 with all-atom simulations. *Proc. Natl. Acad. Sci. USA* **98**, 13014–13018.
- [37] Micheletti, C., Banavar, J. R. & Maritan, A. (2001). Conformations of proteins in equilibrium. *Phys. Rev. Lett.* **87**, Art. No. 088102.
- [38] Portman, J. J., Takada, S. & Wolynes, P. G. (2001). Microscopic theory of protein folding rates. I. Fine structure of the free energy profile and folding routes from a variational approach. *J. Chem. Phys.* **114**, 5069–5081.
- [39] Portman, J. J., Takada, S. & Wolynes, P. G. (2001). Microscopic theory of protein folding rates. II. Local reaction coordinates and chain dynamics. *J. Chem. Phys.* **114**, 5082–5096.
- [40] Cheung, M. S., García, A. E. & Onuchic, J. N. (2002). Protein folding mediated by solvation: Water expulsion and formation of the hydrophobic core occur after the structural collapse. *Proc. Natl. Acad. Sci. USA* **99**, 685–690.
- [41] Jang, H., Hall, C. K. & Zhou, Y. (2002). Folding thermodynamics of model four-strand antiparallel  $\beta$ -sheet proteins. *Biophys. J.* **82**, 646–659.
- [42] Klimov, D. K. & Thirumalai, D. (2002). Stiffness of the distal loop restricts the structural heterogeneity of the transition state ensemble in SH3 domains. *J. Mol. Biol.* **317**, 721–737.
- [43] Makarov, D. E., Keller, C. A., Plaxco, K. W. & Metiu, H. (2002). How the folding rate constant of simple, single-domain proteins depends on the number of native contacts. *Proc. Natl. Acad. Sci. USA* **99**, 3535–3539.

- [44] Micheletti, C., Lattanzi, G. & Maritan, A. (2002). Elastic properties of proteins: Insight on the folding process and evolutionary selection of native structures. *J. Mol. Biol.* **321**, 909–921.
- [45] Zhou, Y. & Linhananta, A. (2002). Thermodynamics of an all-atom off-lattice model of the fragment B of *Staphylococcal* protein A: Implication for the origin of the cooperativity of protein folding. *J. Phys. Chem. B* **106**, 1481–1485.
- [46] Linhananta, A. & Zhou, Y. (2002). The role of sidechain packing and native contact interactions in folding: Discontinuous molecular dynamics folding simulations of an all-atom Gō model of fragment B of *Staphylococcal* protein A. *J. Chem. Phys.* **117**, 8983–8995.
- [47] Kaya, H. & Chan, H. S. (2000). Polymer principles of protein calorimetric two-state cooperativity. *Proteins Struct. Funct. Genet.* **40**, 637–661 [Erratum: **43**, 523 (2001)].
- [48] Kaya, H. & Chan, H. S. (2000). Energetic components of cooperative protein folding. *Phys. Rev. Lett.* **85**, 4823–4826.
- [49] Gō, N. (1999). The consistency principle revisited. In *Old and New Views of Protein Folding*, eds. Kuwajima, K. & Arai, M. (Elsevier, Amsterdam, The Netherlands), pp. 97–105.
- [50] Laughlin, R. B. & Pines, D. (2000). The theory of everything. *Proc. Natl. Acad. Sci. USA* **97**, 28–31.
- [51] Isin, B., Doruker, P. & Bahar, I. (2002). Functional motions of influenza virus hemagglutinin: A structure-based analytical approach. *Biophys. J.* **82**, 569–581.
- [52] Keskin, O., Bahar, I., Flatow, D., Covell, D. G. & Jernigan, R. L. (2002). Molecular mechanisms of chaperonin GroEL-GroES function. *Biochemistry* **41**, 491–501.
- [53] Jacobs, D. J., Rader, A. J., Kuhn, L. A. & Thorpe, M. F. (2001). Protein flexibility prediction using graph theory. *Proteins: Struct. Funct. Genet.* **44**, 150–165.
- [54] Gō, N. (1983). Theoretical studies of protein folding. *Annu. Rev. Biophys. Bioeng.* **12**, 183–210.

- [55] Bryngelson, J. D. & Wolynes, P. G. (1987). Spin glasses and the statistical mechanics of protein folding. *Proc. Natl. Acad. Sci. USA* **84**, 7524–7528.
- [56] Panchenko, A. R., Luthey-Schulten, Z., Cole, R. & Wolynes, P. G. (1997). The foldon universe: A survey of structural similarity and self-recognition of independently folding units. *J. Mol. Biol.* **272**, 95–105.
- [57] Lau, K. F. & Dill, K. A. (1989). A lattice statistical mechanics model of the conformational and sequence spaces of proteins. *Macromolecules* **22**, 3986–3997.
- [58] Chan, H. S. & Dill, K. A. (1991). Sequence space soup of proteins and copolymers. *J. Chem. Phys.* **95**, 3775–3787.
- [59] Shakhnovich, E., Farztdinov, G., Gutin, A. M. & Karplus, M. (1991). Protein folding bottlenecks — a lattice Monte-Carlo simulation. *Phys. Rev. Lett.* **67**, 1665–1668.
- [60] Leopold, P. E., Montal, M. & Onuchic, J. N. (1992). Protein folding funnels — a kinetic approach to the sequence structure relationship. *Proc. Natl. Acad. Sci. USA* **89**, 8721–8725.
- [61] Camacho, C. J. & Thirumalai, D. (1993). Kinetics and thermodynamics of folding in model proteins. *Proc. Natl. Acad. Sci. USA* **90**, 6369–6372.
- [62] Shrivastava, I., Vishveshwara, S., Cieplak, M., Maritan, A. & Banavar, J. R. (1995). Lattice model for rapidly folding protein-like heteropolymers. *Proc. Natl. Acad. Sci. USA* **92**, 9206–9209.
- [63] Plotkin, S. S. (2001). Speeding protein folding beyond the Gō model: How a little frustration sometimes helps. *Proteins Struct. Funct. Genet.* **45**, 337–345.
- [64] Paci, E., Vendruscolo, M. & Karplus, M. (2002). Native and non-native interactions along protein folding and unfolding pathways. *Proteins Struct. Funct. Genet.* **47**, 379–392.
- [65] McCallister, E. L., Alm, E. & Baker, D. (2000). Critical role of  $\beta$ -hairpin formation in protein G folding. *Nature Struct. Biol.* **7**, 669–673.

- [66] Hillson, N., Onuchic, J. N. & García, A. E. (1999). Pressure-induced protein-folding/unfolding kinetics. *Proc. Natl. Acad. Sci. USA* **96**, 14848–14853.
- [67] Chan, H. S. (2000). Modeling protein density of states: Additive hydrophobic effects are insufficient for calorimetric two-state cooperativity. *Proteins Struct. Funct. Genet.* **40**, 543–571.
- [68] Kaya, H. & Chan, H. S. (2002). Towards a consistent modeling of protein thermodynamic and kinetic cooperativity: How applicable is the transition state picture to folding and unfolding? *J. Mol. Biol.* **315**, 899–909.
- [69] Tiktopulo, E. I., Bychkova, V. E., Rička, J. & Ptitsyn, O. B. (1994). Cooperativity of the coil-globule transition in a homopolymer — Microcalorimetric study of poly(*N*-isopropylacrylamide). *Macromolecules* **27**, 2879–2882.
- [70] Matthews, C. R. (1987). Effect of point mutations on the folding of globular proteins. *Methods Enzymol.* **154**, 498–511.
- [71] Gillespie, B. & Plaxco, K. W. (2000). Nonglassy kinetics in the folding of a simple single-domain protein. *Proc. Natl. Acad. Sci. USA* **97**, 12014–12019.
- [72] Jackson, S. E., Moracci, M., elMasry, N., Johnson, C. M. & Fersht, A. R. (1993). Effect of cavity-creating mutations in the hydrophobic core of chymotrypsin inhibitor 2. *Biochemistry* **32**, 11259–11269.
- [73] De Jong, D., Riley, R., Alonso, D. O. V. & Daggett, V. (2002). Probing the energy landscape of protein folding/unfolding transition states. *J. Mol. Biol.* **319**, 229–242.
- [74] Fersht, A. R. & Daggett, V. (2002) Protein folding and unfolding at atomic resolution. *Cell* **108**, (4): 573–582.
- [75] Sobolev, V., Sorokine, A., Prilusky, J., Abola, E. E. & Edelman, M. (1999). Automated analysis of interatomic contacts in proteins. *Bioinformatics* **15**, 327–332.
- [76] Vaiana, S. M., Manno, M., Emanuele, A., Palma-Vittorelli, M. B. & Palma, M. U. (2001). The role of solvent in protein folding and in aggregation. *J. Biol. Phys.* **27**, 133–145.

- [77] Pratt L. R. & Chandler, D. (1977). Theory of the hydrophobic effect. *J. Chem. Phys.* **67**, 3683–3704.
- [78] Geiger, A., Rahman, A. & Stillinger, F. H. (1979). Molecular dynamics study of the hydration of Lennard-Jones solutes. *J. Chem. Phys.* **70**, 263–276.
- [79] Pangali, C., Rao, M. & Berne, B. J. (1979). A Monte Carlo simulation of the hydrophobic interaction. *J. Chem. Phys.* **71**, 2975–2981.
- [80] Guo, C., Cheung, M. S., Levine, H. & Kessler, D. A. (2002). Mechanisms of cooperativity underlying sequence-independent  $\beta$ -sheet formation. *J. Chem. Phys.* **116**, 4353–4365.
- [81] Karanicolas, J. & Brooks, C. L. (2002). The origins of asymmetry in the folding transition states of protein L and protein G. *Protein Sci.* **11**, 2351–2361.
- [82] Roux, B. & Simonson, T. (1999). Implicit solvent models. *Biophys. Chem.* **78**, 1–20.
- [83] Shimizu, S. & Chan, H. S. (2002). Anti-cooperativity and cooperativity in hydrophobic interactions: Three-body free energy landscapes and comparison with implicit-solvent potential functions for proteins. *Proteins Struct. Funct. Genet.* **48**, 15–30. [Erratum: **49**, 294 (2002)].
- [84] Shimizu, S. & Chan, H. S. (2000). Temperature dependence of hydrophobic interactions: A mean force perspective, effects of water density, and non-additivity of thermodynamic signatures. *J. Chem. Phys.* **113**, 4683–4700. [Erratum: **116**, 8636 (2002)].
- [85] Shimizu, S. & Chan, H. S. (2001). Configuration-dependent heat capacity of pairwise hydrophobic interactions. *J. Am. Chem. Soc.* **123**, 2083–2084.
- [86] Ghosh, T., García, A. E. & Garde, S. (2002). Enthalpy and entropy contributions to the pressure dependence of hydrophobic interactions. *J. Chem. Phys.* **116**, 2480–2486.
- [87] Berendsen, H. J. C., Postma, J. P. M., van Gunsteren, W. F., DiNola, A. & Haak, J. R. (1984). Molecular dynamics with coupling to an external bath. *J. Chem. Phys.* **81**, 3684–3690.

- [88] Guo, Z. & Thirumalai, D. (1995). Kinetics of protein folding: Nucleation mechanism, time scales, and pathways. *Biopolymers* **36**, 83–102.
- [89] Veitshans, T., Klimov, D. & Thirumalai, D. (1997). Protein folding kinetics: Timescales, pathways and energy landscapes in terms of sequence-dependent properties. *Fold. Des.* **2**, 1–22.
- [90] Allen, M. P. & Tildesley, D. J. (1987). *Computer Simulation of Liquids*. Oxford University Press, Oxford, UK.
- [91] Swope, W. C., Andersen, H. C., Berens, P. H. & Wilson, K. R. (1982). A computer simulation method for the calculation of equilibrium constants for the formation of physical clusters of molecules: Application to small water clusters. *J. Chem. Phys.* **76**, 637–649.
- [92] Fersht, A. R. (1997). Nucleation mechanisms in protein folding. *Curr. Opin. Struct. Biol.* **7**, 3–9.
- [93] Chu, R.-A. & Bai, Y. (2002). Lack of definable nucleation sites in the rate-limiting transition state of barnase under native conditions. *J. Mol. Biol.* **315**, 759–770.
- [94] Yang, D., Mok, Y. K., Forman-Kay, J. D., Farrow, N. A. & Kay, L. E. (1997). Contributions to protein entropy and heat capacity from bond vector motions measured by NMR spin relaxation. *J. Mol. Biol.* **272**, 790–804.
- [95] Jackson, S. A. & Fersht, A. R. (1991). Folding of chymotrypsin inhibitor 2. 1. Evidence for a two-state transition. *Biochemistry* **30**, 10428–10435.
- [96] Cui, Y., Wong, W. H., Bornberg-Bauer, E. & Chan, H. S. (2002). Recombinatoric exploration of novel folded structures: A heteropolymer-based model of protein evolutionary landscapes. *Proc. Natl. Acad. Sci. USA* **99**, 809–814.
- [97] Chan, H. S. & Bornberg-Bauer, E. (2002). Perspectives on protein evolution from simple exact models. *Applied Bioinformatics*, in press.
- [98] Chan, H. S. & Dill, K. A. (1998). Protein folding in the landscape perspective: Chevron plots and non-Arrhenius kinetics. *Proteins Struct. Funct. Genet.* **30**, 2–33.



- [99] Bakk, A., Høye, J. S., Hansen, A., Sneppen, K. & Jensen, M. H. (2000). Pathways in two-state protein folding. *Biophys. J.* **79**, 2722–2727.
- [100] Uversky, V. N. & Fink, A. L. (2002). The chicken-egg scenario of protein folding revisited. *FEBS Lett.* **515**, 79–83.
- [101] Creamer, T. P. & Rose, G. D. (1994).  $\alpha$ -Helix-forming propensities in peptides and proteins. *Proteins Struct. Funct. Genet.* **19**, 85–97.
- [102] Chan, H.S. (1998). Modelling protein folding by Monte Carlo dynamics: Chevron plots, chevron rollover, and non-Arrhenius kinetics. In *Monte Carlo Approach to Biopolymers and Protein Folding* (Grassberger, P., Barkema, G.T. & Nadler, W., eds) pp. 29–44, World Scientific, Singapore.
- [103] Wallqvist, A., Covell, D. G., Thirumalai, D. (1998). Hydrophobic interactions in aqueous urea solutions with implications for the mechanism of protein denaturation. *J. Am. Chem. Soc.* **120**, 427–428.
- [104] Crippen, G. M. (2001). A Gaussian statistical mechanical model for the equilibrium thermodynamics of barnase folding. *J. Mol. Biol.* **306**, 565–573.
- [105] Ikeguchi, M., Nakamura S, Shimizu, K. (2001). Molecular dynamics study on hydrophobic effects in aqueous urea solutions. *J. Am. Chem. Soc.* **123**, 677–682.
- [106] Shimizu, S. & Chan, H. S. (2002). Origins of protein denatured states compactness and hydrophobic clustering in aqueous urea: Inferences from nonpolar potentials of mean force. *Proteins Struct. Funct. Genet.* **49**, 560–566.
- [107] Englander, S. W., Mayne, L., Bai, Y. & Sosnick, T. R. (1997). Hydrogen exchange: The modern legacy of Linderstrøm-Lang. *Protein Sci.* **6**, 1101–1109.
- [108] Kim, K. S. & Woodward, C. (1993). Protein internal flexibility and global stability: Effect of urea on hydrogen-exchange rates of bovine pancreatic trypsin inhibitor. *Biochemistry* **32**, 9609–9613.
- [109] Bai, Y., Sosnick, T. R., Mayne, L. & Englander, S. W. (1995). Protein folding intermediates: Native-state hydrogen exchange. *Science* **269**, 192–197.

- [110] Llinás, M., Gillespie, B., Dahlquist, F. W. & Marqusee, S. (1999). The energetics of T4 lysozyme reveal a hierarchy of conformations. *Nature Struct. Biol.* **6**, 1072–1078.
- [111] Klimov, D. K. & Thirumalai, D. (2002). Is there a unique melting temperature for two-state proteins? *J. Comput. Chem.* **23**, 161–165.
- [112] Kuhlman, B., Luisi, D. L., Evans, P. A. & Raleigh, D. P. (1998). Global analysis of the effects of temperature and denaturant on the folding and unfolding kinetics of the N-terminal domain of the protein L9. *J. Mol. Biol.* **284**, 1661–1670.
- [113] Houry, W. A., Rothwarf, D. M. & Scheraga, H. A. (1995). The nature of the initial step in the conformational folding of disulphide-intact ribonuclease A. *Nature Struct. Biol.* **2**, 495–503.
- [114] Oliveberg, M., Tan, Y. J. & Fersht, A. R. (1995). Negative activation enthalpies in the kinetics of protein folding. *Proc. Natl. Acad. Sci. USA* **92**, 8926–8929.
- [115] Abkevich, V. I., Gutin, A. M. & Shakhnovich, E. I. (1994). Free energy landscape for protein folding kinetics: Intermediates, traps, and multiple pathways in theory and lattice model simulations. *J. Chem. Phys.* **101**, 6052–6062.
- [116] Nymeyer, H., Socci, N. D. & Onuchic, J. N. (2000). Landscape approaches for determining the ensemble of folding transition states: Success and failure hinge on the degree of frustration. *Proc. Natl. Acad. Sci. USA* **97**, 634–639.
- [117] Socci, N. D., Onuchic, J. N. & Wolynes, P. G. (1996). Diffusive dynamics of the reaction coordinate for protein folding funnels. *J. Chem. Phys.* **104**, 5860–5868.
- [118] Fersht, A. R., Matouschek, A. & Serrano, L. (1992). The folding of an enzyme. I. Theory of protein engineering analysis of stability and pathway of protein folding. *J. Mol. Biol.* **224**, 771–782.
- [119] Schuler, B., Lipman, E. A. & Eaton, W. A. (2002). Probing the free-energy surface for protein folding with single-molecule fluorescence spectroscopy. *Nature* **419**, 743–747.
- [120] Matouschek, A., Kellis, J. T., Serrano, L., Bycroft, M. & Fersht, A. R. (1990). Characterizing transient folding intermediates by protein engineering. *Nature* **346**, 440–445.

- [121] Li, R., Battiste, J. L. & Woodward, C. (2002). Native-like interactions favored in the unfolded bovine pancreatic trypsin inhibitor have different roles in folding. *Biochemistry* **41**, 2246–2253.
- [122] Oliveberg, M. (1998). Alternative explanations for “multistate” kinetics in protein folding: Transient aggregation and changing transition-state ensembles. *Acc. Chem. Res.* **31**, 765–772.
- [123] Parker, M. J. & Marqusee, S. (1999). The cooperativity of burst phase reactions explored. *J. Mol. Biol.* **293**, 1195–1210.
- [124] Du, R., Pande, V. S., Grosberg, A. Yu., Tanaka, T. & Shakhnovich, E. I. (1998). On the transition coordinate for protein folding. *J. Chem. Phys.* **108**, 334–350.
- [125] Sabelko, J., Ervin, J. & Gruebele, M. (1999). Observation of strange kinetics in protein folding. *Proc. Natl. Acad. Sci. USA* **96**, 6031–6036.
- [126] Eaton, W. A. (1999). Searching for “downhill scenarios” in protein folding. *Proc. Natl. Acad. Sci. USA* **96**, 5897–5899.
- [127] Lazaridis, T. & Karplus, M. (1999). Effective energy functions for proteins in solution. *Proteins Struct. Funct. Genet.* **35**, 133–152.
- [128] Day, R., Bennion, B. J., Ham, S. & Daggett, V. (2002). Increasing temperature accelerates protein unfolding without changing the pathway of unfolding. *J. Mol. Biol.* **322**, 189–203.
- [129] ten Wolde, P. R. & Chandler, D. (2002). Drying-induced hydrophobic polymer collapse. *Proc. Natl. Acad. Sci. USA* **99**, 6539–6543.
- [130] Fan, K., Wang, J. & Wang, W. (2001). Modeling two-state cooperativity in protein folding. *Phys. Rev. E* **64**, Art. No. 041907.
- [131] Crippen, G. M. & Chhajer, M. (2002). Lattice models of protein folding permitting disordered native states. *J. Chem. Phys.* **116**, 2261–2268.

**Table 1**

unfolding					folding				
$\epsilon$	NCS1		NCS2		$\epsilon$	NCS1		NCS2	
	MFPT/ $10^5$	$N_t$	MFPT/ $10^5$	$N_t$		MFPT/ $10^5$	$N_t$	MFPT/ $10^5$	$N_t$
0.60	0.1734	100	0.1763	100	1.00	0.6905	100	0.9250	100
0.65	0.2472	100	0.2547	100	0.95	0.9534	100	1.1668	100
0.70	0.3825	100	0.4212	100	0.90	1.4646	100	1.3102	100
0.75	0.7807	100	0.8950	100	0.89	1.5062	100	1.3865	100
0.77	1.2540	1100	1.9052	1100	0.88	1.8175	1100	1.5577	1100
0.78	1.7684	100	2.8292	100	0.87	2.1760	100	2.0039	100
0.79	2.4983	100	4.7346	100	0.86	2.2865	100	2.3725	100
0.80	2.3120	100	8.0901	100	0.85	3.0018	100	2.7999	100
0.82	3.4755	100	42.737	100	0.84	4.2971	100	4.0108	100
—	—	—	—	—	0.83	4.6969	100	5.1892	100
—	—	—	—	—	0.82	7.9260	100	7.3979	100
—	—	—	—	—	0.80	20.278	100	17.844	100

**Table 1.** Number of trajectories  $N_t$  used in the present study to determine the MFPT of folding and unfolding for the NCS1 and NCS2 without-solvation models ( $T = 0.82$ , Figure 7). Each MFPT listed is the average (arithmetic mean) over  $N_t$  first passage times for the given interaction strength  $\epsilon$ . Time is measured from the start of a given simulation at  $t = 0$  in units of  $\delta t$  (see text).

**Table 2**

unfolding					folding				
$\epsilon$	NCS1		NCS2		$\epsilon$	NCS1		NCS2	
	MFPT/ $10^5$	$N_t$	MFPT/ $10^5$	$N_t$		MFPT/ $10^5$	$N_t$	MFPT/ $10^5$	$N_t$
0.70	0.1804	100	0.1856	100	1.30	1.0080	100	0.9121	100
0.75	0.2450	100	0.2730	100	1.25	1.1324	100	1.0924	100
0.80	0.3362	100	0.3759	100	1.20	1.4063	100	1.0754	100
0.83	0.4489	100	0.5304	100	1.18	1.4840	100	1.2380	100
0.85	0.5653	1100	0.6950	1940	1.15	1.7905	1100	1.6733	1097
0.88	0.9161	100	1.2724	100	1.13	2.3409	100	1.6971	100
0.90	1.3364	100	2.3473	100	1.10	2.8513	100	2.2875	100
0.93	2.3120	100	6.5846	100	1.08	4.0404	100	3.0059	100
0.95	4.7098	100	15.767	100	1.05	6.8365	100	4.8426	100
0.97	9.4389	75	40.261	45	1.03	10.385	100	9.6890	100
0.98	16.268	91	42.673	20	1.00	43.174	52	25.440	60
0.99	—	—	71.042	15	0.98	—	—	110.78	24
1.00	51.148	18	262.14	7	0.97	—	—	349.46	14

**Table 2.** Same as Table 1, but for the without-solvation-SSR models ( $T = 0.64$ , Figure 8).

**Table 3**

unfolding					folding				
$\epsilon$	NCS1		NCS2		$\epsilon$	NCS1		NCS2	
	MFPT/ $10^5$	$N_t$	MFPT/ $10^5$	$N_t$		MFPT/ $10^5$	$N_t$	MFPT/ $10^5$	$N_t$
0.40	0.5559	600	0.6549	500	1.50	1.2196	100	2.1393	150
0.50	0.8419	126	1.5782	137	1.40	2.4237	108	3.5297	176
0.60	1.6697	111	7.2719	121	1.30	3.9479	117	5.5725	176
0.65	2.7900	103	17.122	50	1.25	5.4452	107	8.7000	85
0.70	5.4940	1100	44.590	205	1.20	6.8649	112	11.766	50
0.75	8.4002	120	104.18	34	1.18	8.7936	119	—	—
0.80	15.463	91	293.56	26	1.15	10.823	52	30.141	42
0.83	26.101	51	—	—	1.10	19.633	427	48.000	205
0.85	42.512	74	722.32	15	1.08	20.336	36	—	—
0.90	119.01	32	1224.2	6	1.05	41.682	63	143.75	24
0.92	—	—	1922.0	4	1.03	43.365	56	166.15	20
0.93	168.05	24	—	—	1.00	75.048	52	330.35	28
0.95	216.32	37	—	—	0.97	93.742	40	444.98	7
					0.95	132.12	37	783.56	6
					0.90	—	—	1519.4	3

**Table 3.** Same as Table 1, but for the with-solvation models ( $T = 0.82$ , Figure 9).

## Figure Captions

**Figure 1.** Native contact maps of the 64-residue truncated form of chymotrypsin inhibitor 2 (2ci2) used in the present investigation. (a) Contact maps for the native contact sets NCS1 (green dots) and NCS2 (red dots) as defined in the text. Numbering of amino acids in these maps is initialized at residue 20 of the full-length 83-residue CI2; i.e., residue 1 in (a) corresponds to Leu 20 in the untruncated protein. (b, c, d) Similarities and differences between native contact maps. Contact pairs are indicated by color lines joining  $C_\alpha$  positions along the backbone (black trace). (b) Contacts shared by NCS1 and NCS2. (c) Contacts in NCS1 but not in NCS2. (d) Contacts in NCS2 but not in NCS1.

**Figure 2.** Different native contact definitions. Amino acid numbering here corresponds to that of the full-length CI2, i.e., numbering in this figure equals to that in Fig. 1a plus 19. The red contact belongs to NCS2 but not NCS1. This pair of residues has a  $C_\alpha$ - $C_\alpha$  distance of 11.24 Å, with closest atomic separation between the residues equals 4.3 Å. The green contact belongs to NCS1 but not NCS2. The  $C_\alpha$ - $C_\alpha$  distance between this pair of residue is 5.36 Å.

**Figure 3.** (a) Model with-solvation interactions between two amino acid residues belonging to a given native contact pair in the present study (defined by either NCS1 or NCS2);  $r$  is their  $C_\alpha$ - $C_\alpha$  separation. The potential energy  $U(r)$ , shown here and in part (b) in units of  $\epsilon$ , depends also on the native  $C_\alpha$ - $C_\alpha$  distance  $r'$  of a given contact in the PDB structure. The  $r'$  values shown in this figure are only for illustrative purposes. They do not correspond to actual contacts in the present NCS1 or NCS2 models (see text).  $U(r)$  here is defined by the functional form of Cheung et al.<sup>40</sup> with  $k = 6$ ,  $n = 2$ ,  $m = 3$ ,  $\epsilon' = 0.2\epsilon$ , and  $\epsilon'' = 0.1\epsilon$ , where  $k$ ,  $n$ , and  $m$  parametrize the functional form for  $r < r'$ ,  $r' \leq r < r^\dagger$  and  $r \geq r^\dagger$ , respectively (e.g., the excluded volume repulsion  $\sim r^{-2k}$ , see equation on page 689 of ref. 40 for details),  $\epsilon'$  is the depth of water-separated minimum, and  $\epsilon''$  is the height of the desolvation peak. The two potential functions shown in (a) are for  $r' = 4.0$  Å (left) and  $r' = 6.5$  Å (right). The cartoons (for  $r' = 6.5$  Å) illustrate contact and water-separated minima configurations,<sup>40,83</sup> where a water molecule is depicted as a solid circle of diameter  $\approx 3$  Å. (b) With-solvation native potential for  $r' = 3.8$  Å in the present study (as labeled) is compared with: (i) The  $r' = 3.8$  Å functional form of Cheung et al. with the same values for  $k$ ,  $n$ ,  $m$ ,

and  $\epsilon$  as in (a), but with  $\epsilon' = \epsilon/3$  and  $\epsilon'' = 5\epsilon/9$ . **(ii)** The explicit-water simulated methane-methane PMF at 25° C under atmospheric pressure obtained by Shimizu and Chan,<sup>83</sup> in a unit such that the free energy at contact equals  $-\epsilon = -1$ . **(LJ)** The 10–12 Lennard-Jones without-solvation potential  $\epsilon[5(r'/r)^{12} - 6(r'/r)^{10}]$  (as in equation 1) with  $r' = 3.8 \text{ \AA}$ . **(SSR)** The corresponding LJ cutoff at  $1.2r'$  in without-solvation-SSR models.

**Figure 4.** Free energy profiles for NCS1 (dashed curves) and NCS2 (solid curves), using native contact potentials without (a, b) and with (c) desolvation barriers. (a) is for without-solvation models that use the full spatial range of the LJ terms whereas (b) is for without-solvation-SSR models with LJ cutoffs. The variable  $Q$  is the number of native contacts in a conformation divided by the number of contacts in the native conformation of the given model.  $P(Q)$  is the normalized population distribution over  $Q$ . The  $-\ln P(Q)$  profiles are computed at each model’s approximate transition midpoint: (a) at  $\epsilon/k_B T = 0.988$  and  $0.988$  for the NCS1 and NCS2 without-solvation models, (b) at  $\epsilon/k_B T = 1.563$  and  $1.547$  for the NCS1 and NCS2 without-solvation-SSR models, and (c) at  $\epsilon/k_B T = 1.165$  and  $1.098$  for the NCS1 and NCS2 with-solvation models. For without-solvation models in (a) and (b), the condition for contact is  $r \leq 1.2r'$ , as in ref. 32. For with-solvation models in (c), a pair of residues is defined to be in contact when  $r \leq r^\dagger = (r' + r'')/2$ , i.e., when the  $C_\alpha$ – $C_\alpha$  distance  $r$  is within the contact basin ( $r$  not larger than that of the desolvation peak), as in ref. 40.

**Figure 5.** Thermodynamic cooperativity. Heat capacity as a function of temperature is shown for seven models: (i) the contact-dominant model described in the text, (ii) NCS1 and (iii) NCS2 without-solvation-SSR models, (iv) NCS1 and (v) NCS2 with-solvation models, and (vi) NCS1 and (vii) NCS2 without-solvation models. Vertical dotted lines correspond to the transition midpoints marked in Figures 7–9. The computed van’t Hoff to calorimetric enthalpy ratios (defined in ref. 47) for these models with no baseline subtractions are, respectively,  $\kappa_2 = 0.30, 0.57, 0.61, 0.56, 0.63, 0.46,$  and  $0.50$ . The corresponding ratios after subtracting the empirical baselines (shown in the figure) are  $\kappa_2^{(s)} = 0.33, 0.98, 1.00, 1.00, 1.01, 0.97,$  and  $0.99$ . The unit of every heat capacity scan plotted is for interaction strength  $\epsilon = 1$ . Each scan was calculated from the density of states estimated by histogram techniques.<sup>32,47</sup> The sampling simulations were conducted at temperature  $T$  and  $\epsilon$  values chosen around each model’s transition



midpoint to efficiently cover both the folded and unfolded regions of the conformational space. For (i) – (vii),  $T = 0.32, 0.64, 0.64, 0.82, 0.82, 0.82$ , and  $0.82$ , respectively, and  $\epsilon = 1.0, 1.0, 1.0, 0.955, 0.90, 0.81$ , and  $0.81$  were used.

**Figure 6.** Signatures of two-state thermodynamics and sharp kinetic transitions between states in the with-solvation NCS2 model at  $T = 0.82$ . Time evolution is monitored by snapshots taken at every  $400\delta t$  during the simulations. (a) A folding/unfolding trajectory near the transition midpoint of this model at  $\epsilon = 0.90$  ( $-\epsilon/k_B T = -1.098$ ,  $\Delta G_u/k_B T = 0.68$ ). (b) A trajectory showing transient unfolding under moderately native conditions at  $\epsilon = 0.92$  ( $-\epsilon/k_B T = -1.122$ ,  $\Delta G_u/k_B T = 2.70$ ). (c) Scatter plot of potential energy  $V_{\text{total}}^{(S)}$  versus kinetic energy of the model protein (sum of  $mv^2/2$  over all  $C_\alpha$  positions) for the trajectory in (a). Each dot represents a snapshot. The first 11 snapshots are connected by line segments to highlight the initial pre-equilibration process. The average kinetic energy is equal to 78.9. (d) is the corresponding scatter plot of potential energy versus  $Q$  for the trajectory in (a) and (c).

**Figure 7.** Folding/unfolding kinetics and thermodynamics of the without-solvation NCS1 (squares, dashed curves) and NCS2 (circles, solid curves) models at  $T = 0.82$ . **Upper panel:** Chevron plots of negative natural logarithm of folding (filled symbols) and unfolding (open symbols) MFPT data from Table 1. The curves are guides for the eye. Unfolding simulations start with the native conformation; FPT is defined by the chain having  $\leq 25$  native contacts. Folding simulations start with randomly generated open conformations with  $Q \approx 10\%$ , FPT is defined by the chain achieving a  $Q$  value larger than or equal to that of the native free energy minima on the free energy profiles in Figure 4A, i.e.,  $Q \geq 112/137$  for NCS1 and  $Q \geq 120/142$  for NCS2. **Lower panel:** The free energy of unfolding  $\Delta G_u$  in units of  $k_B T$  for each of the two models (dashed lines: NCS1, solid lines: NCS2) is the natural logarithm of the Boltzmann weight (population) of the folded state minus that of the denatured chain population with  $\leq 35$  native contacts (upper curves) or that with  $\leq 70$  native contacts (lower curves). Conformations with  $\geq 100$  out of 137, and  $\geq 105$  out of 142 native contacts (corresponding approximately to  $Q \geq 0.73$  around the native minima in Figure 4A) are taken to be the folded states, respectively, of the NCS1 and NCS2 models. Stability curves shown are obtained by histogram techniques from simulations at  $\epsilon = 0.80$  and  $0.81$  for NCS1, and at  $\epsilon = 0.80$ ,

0.81, and 0.82 for NCS2. The vertical dotted line marks the midpoint  $-\epsilon/k_B T$  values at which  $\Delta G_u = 0$  for the two models. The V-shaped dashed-dot lines in the upper panel is an hypothetical simple two-state chevron plot that would be consistent with the models' approximately linear thermodynamic stability curves in the lower panel. Note that the quasis-linear stability curves of the two models have approximately the same slope.

**Figure 8.** Same as Figure 7 but for the without-solvation-SSR models at  $T = 0.64$ . Simulation details not identical to that in Figure 7 are as follows. **Upper panel:** MFPTs are from Table 2. Here folding FPT is defined by the chain achieving  $Q = 1$ . **Lower panel:** Stability curves are given by the natural logarithm of the Boltzmann weight (population) of the folded state minus that of the denatured chain population with  $\leq 35$  native contacts (upper curves) or that with  $\leq 80$  native contacts (lower curves). Conformations with 132 out of 137, and 137 out of 142 native contacts (corresponding to the native minima on the free energy profiles in Figure 4B) are taken to be the folded states, respectively, of the NCS1 and NCS2 models. The  $\Delta G_u/k_B T$  stability curves remain essentially unchanged if the thermodynamic definitions for the folded states of these models are extended to  $Q \geq 132/137$  for NCS1 and  $Q \geq 137/142$  for NCS2. Stability curves shown are obtained by histogram techniques from simulations at  $\epsilon = 0.97, 0.98, 0.99$ , and 1.00 for NCS1, and at  $\epsilon = 0.99, 1.00$ , and 1.01 as well as confirmed by simulations at several temperatures other than  $T = 0.64$  for NCS2.

**Figure 9.** Same as Figure 8 but for the with-solvation models at  $T = 0.82$ . Simulation details not identical to that in Figure 8 are as follows. **Upper panel:** MFPTs are from the  $0.6 \leq \epsilon \leq 1.30$  entries in Table 3. Otherwise the kinetic definitions of folding and unfolding are the same as that in Figure 8. **Lower panel:** Stability curves are given by the natural logarithm of the Boltzmann weight of the folded state minus that of the denatured chain population with  $\leq 30$  native contacts (upper curves) or that with  $\leq 80$  (lower curves). The folded state is defined here by conformations with exactly  $Q = 1$  (c.f. Figure 4C). The stability curves are obtained by histogram techniques from simulations at  $\epsilon = 0.955$  and 0.96 for NCS1, and at  $\epsilon = 0.90$  for NCS2.

**Figure 10.** Approximate single exponential folding kinetics indicated by first passage time (FPT) distributions.  $P(t)\Delta t$  is the fraction of trajectories with  $t - \Delta t/2 <$

$\text{FPT} \leq t + \Delta t/2$ . (a) The FPT distribution among the 1,097 folding trajectories under strongly native conditions at  $-\epsilon/k_{\text{B}}T = -1.80$  in the NCS2 without-solvation-SSR model ( $\epsilon = 1.15$  entry in Table 2) is shown for bin sizes  $\Delta t = 10^5$  (filled circles) and  $\Delta t = 2 \times 10^4$  (open circles). The solid line is the least-square fit through the  $\Delta t = 10^5$  data points. (b) Included for comparison is the FPT distribution among the 1,080 folding trajectories of the three-dimensional lattice model described on page 903 of Kaya and Chan<sup>68</sup> with  $\epsilon/k_{\text{B}}T = -1.72$  and  $\Delta t = 10^6$ ;  $t$  is the number of Monte Carlo time steps. The solid line is the least-square fit (correlation coefficient  $r = 0.95$ ) through the data points shown in the main figure; 20 trajectories that give rise to a long-FPT tail in the full distribution (inset) are excluded from this fit. The dashed line is equation 6 with  $\ln(\text{MFPT}) = 16.25$  from ref. 68;  $t_0$  was taken to be zero for this lattice case.

**Figure 11.** Approximate single-exponential folding and unfolding kinetics. FPT distributions are presented as in Figure 10A. Solid lines are least-square fits through the data points shown. Numbers of trajectories in the distributions are given in Tables 1–3. Unfolding and folding data using NCS1 (or NCS2) are plotted, respectively, by open and filled squares (or circles). (a) Without-solvation models. (b) Without-solvation-SSR models. The NCS2 folding plot here is identical to the  $\Delta t = 10^5$  case in Figure 10A. (c) With-solvation models. The  $\epsilon$  values for NCS1 unfolding, folding, NCS2 unfolding, folding, and the corresponding  $\Delta t$  bin sizes for these different models are, respectively, (a)  $\epsilon = 0.77, 0.88, 0.77, 0.88, \Delta t/10^5 = 0.84, 1.4, 1.5, 1.2$ ; (b)  $\epsilon = 0.85, 1.15, 0.85, 1.15, \Delta t/10^5 = 0.21, 1.3, 0.4, 1.0$ ; (c)  $\epsilon = 0.70, 1.10, 0.70, 1.10, \Delta t/10^6 = 0.45, 2.0, 4.6, 5.5$ .

**Figure 12.** Front factor analyses. (a – c): Free energy profiles for the NCS2 without-solvation (a), without-solvation-SSR (b) and with-solvation (c) models at the  $\epsilon$  values indicated (c.f. Figure 4). These plots are obtained from Boltzmann distributions computed by histogram techniques. Where appropriate, different line styles are used for profiles at different  $\epsilon$  values for clarity. Shaded areas are examples of unfolded, transition, and folded state regions considered (see text). (d) Correlations between rates and activation free energies deduced from free energy profiles are analyzed as in ref. 68. The vertical variable is given by  $\ln F = -\ln(\text{MFPT}) + \Delta G^\ddagger/k_{\text{B}}T$  (equation 7). In the present analysis,  $\Delta G^\ddagger(\epsilon, T)/k_{\text{B}}T = -\ln[P(60/142 \leq Q \leq 80/142)/P(Q \geq 105/142)]$  (open triangles, without-solvation unfolding),  $-\ln[P(60/142 \leq Q \leq 80/142)/P(Q \leq 35/142)]$  (filled

triangles, without-solvation folding),  $-\ln[P(75/142 \leq Q \leq 95/142)/P(Q = 137/142)]$  (open squares, without-solvation-SSR unfolding),  $-\ln[P(75/142 \leq Q \leq 95/142)/P(Q \leq 25/142)]$  (filled squares, without-solvation-SSR folding),  $-\ln[P(70/142 \leq Q \leq 95/142)/P(Q = 1)]$  (open circles, with-solvation unfolding), and  $-\ln[P(70/142 \leq Q \leq 95/142)/P(Q \leq 25/142)]$  (filled circles, with-solvation folding). The middle shaded regions in (a – c) correspond to the transition-state regions used in the analysis in (d). NCS1 models have similar trends (data not shown).

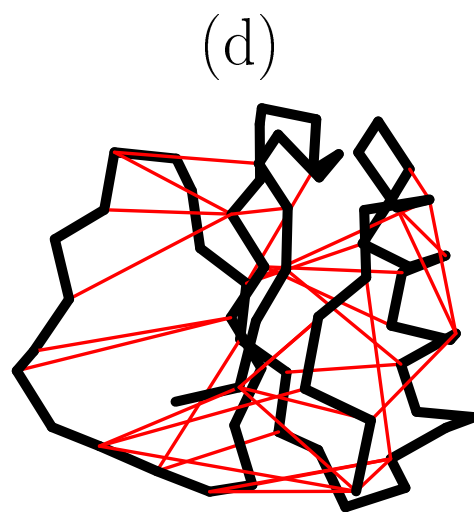
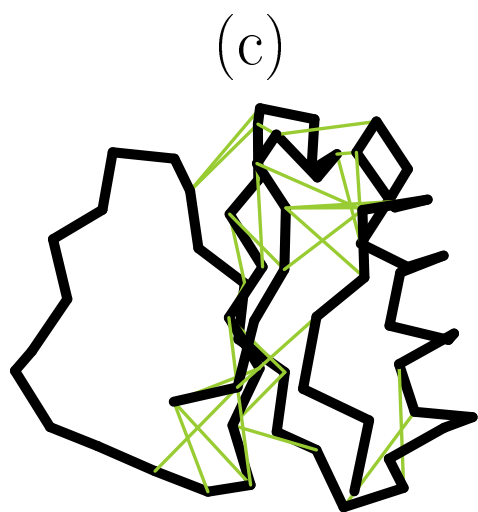
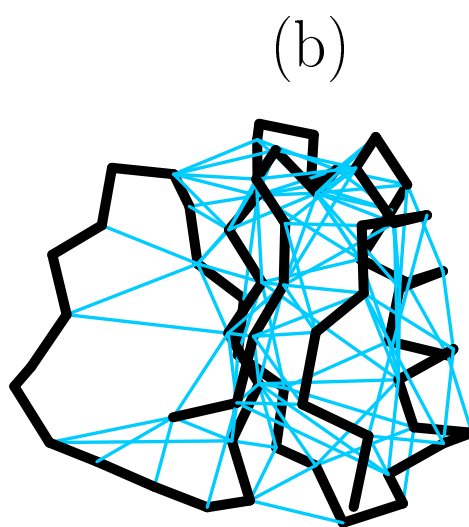
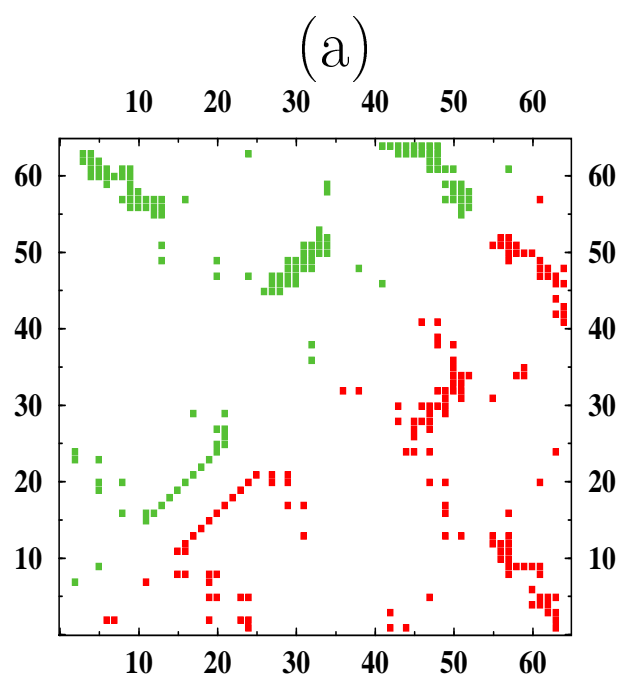
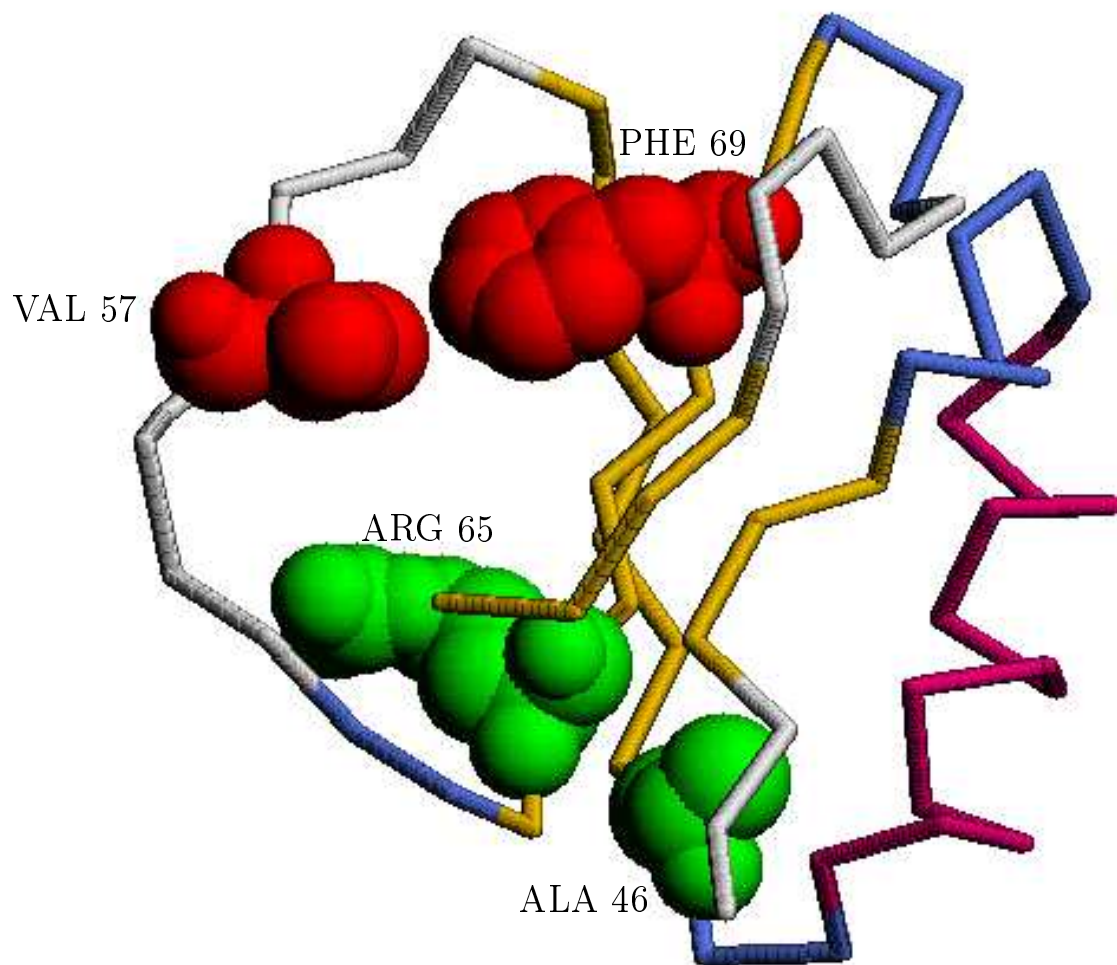
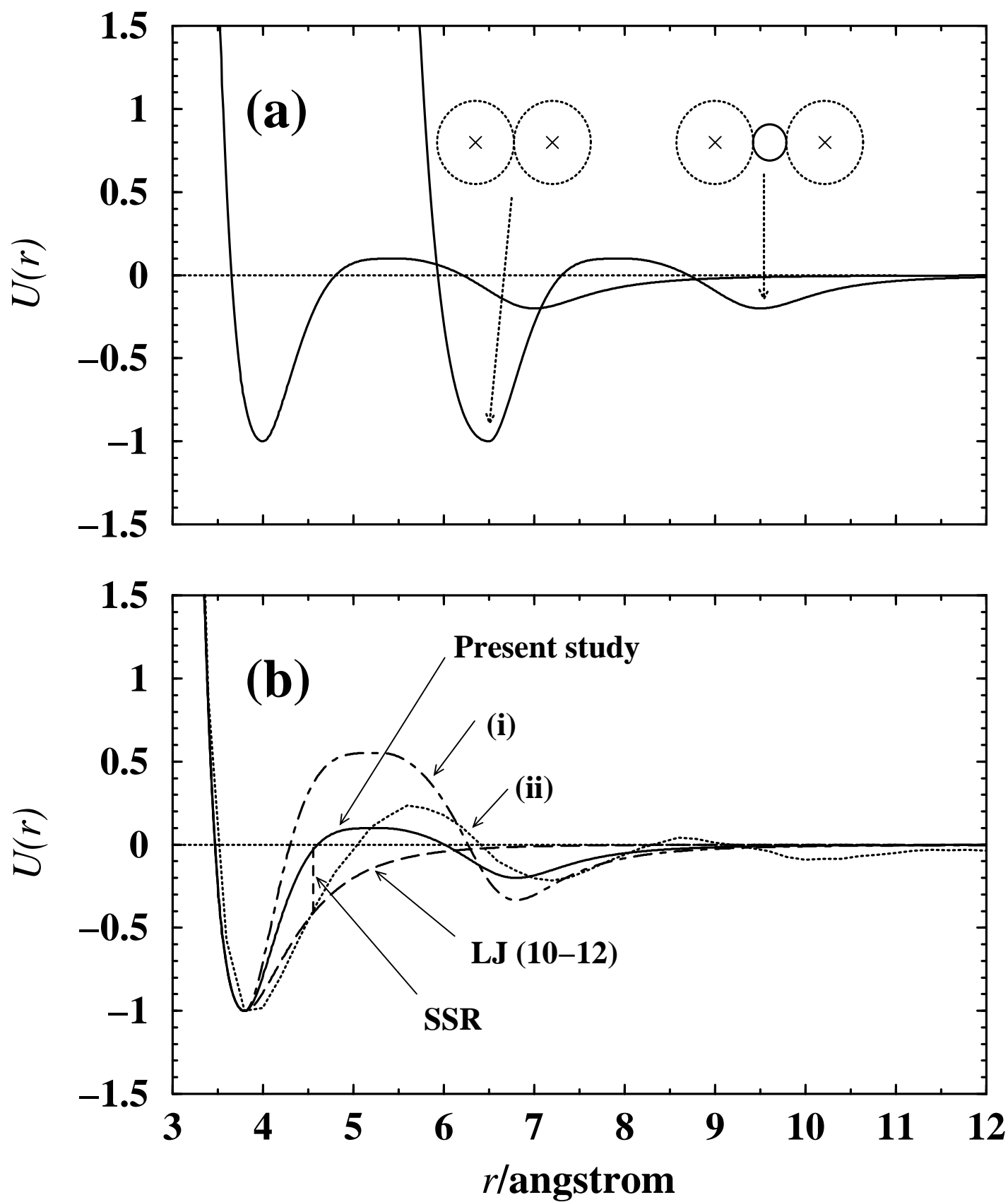


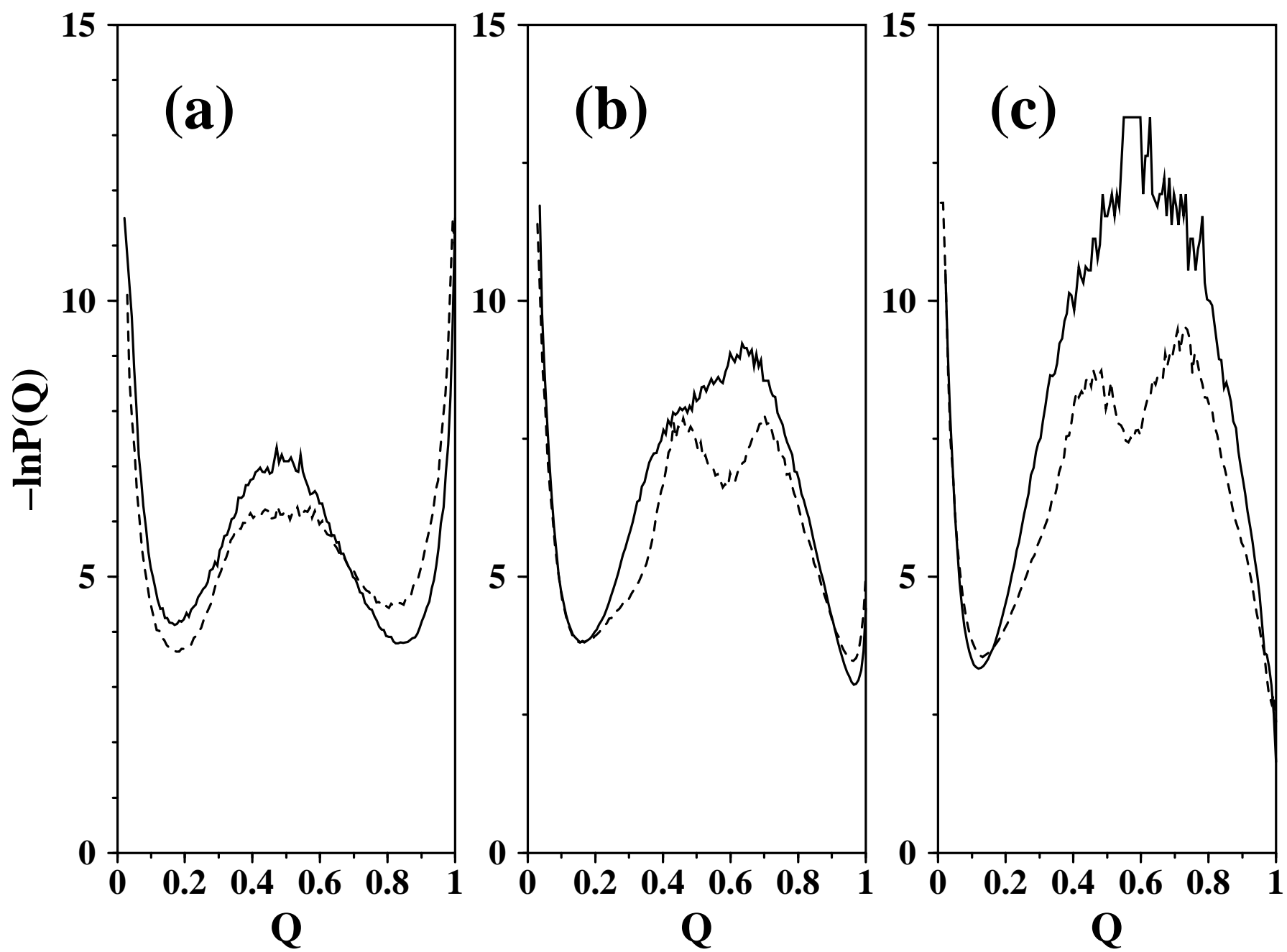
Fig.1



**Fig.3**

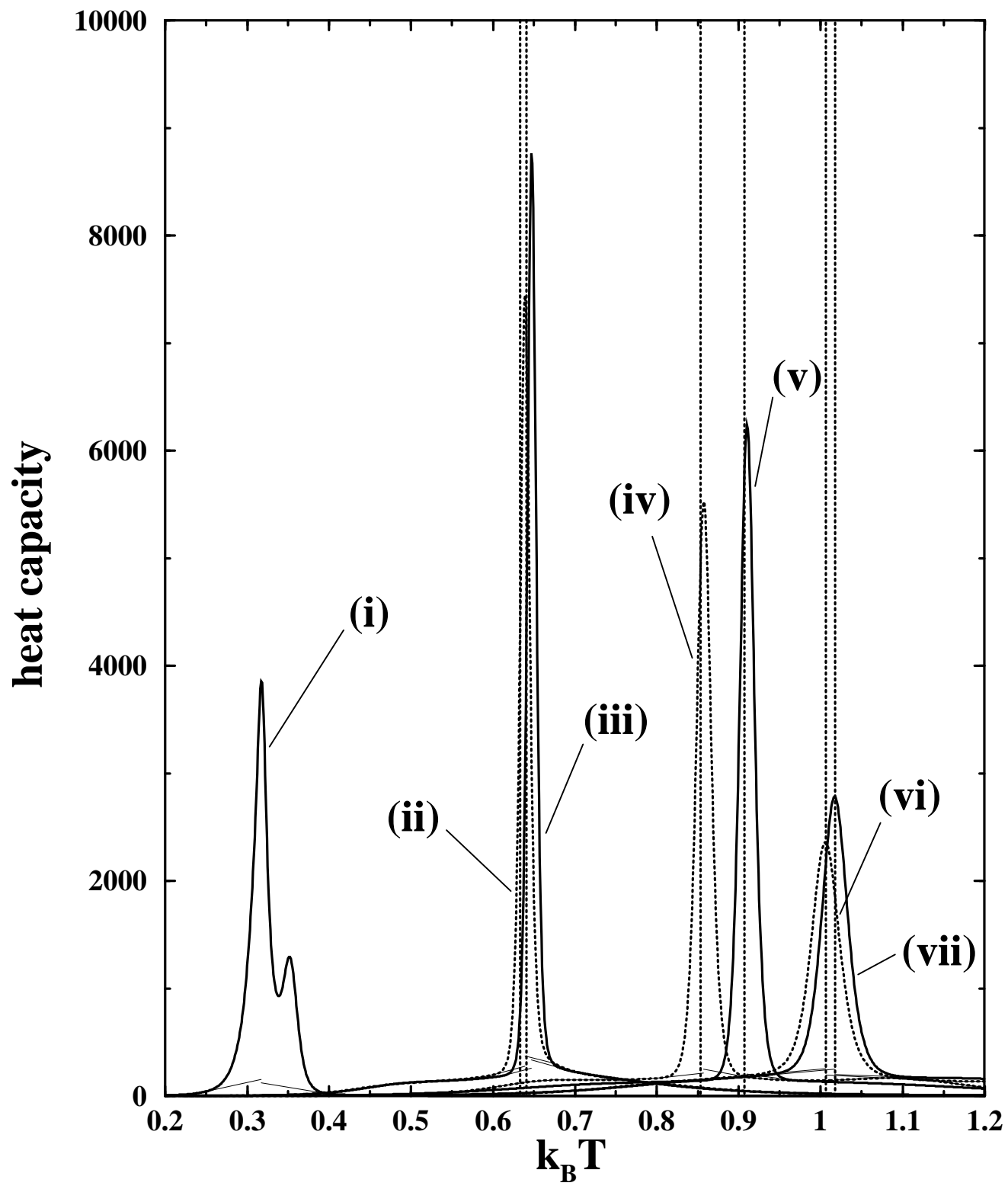


**Fig.4**





**Fig.5**



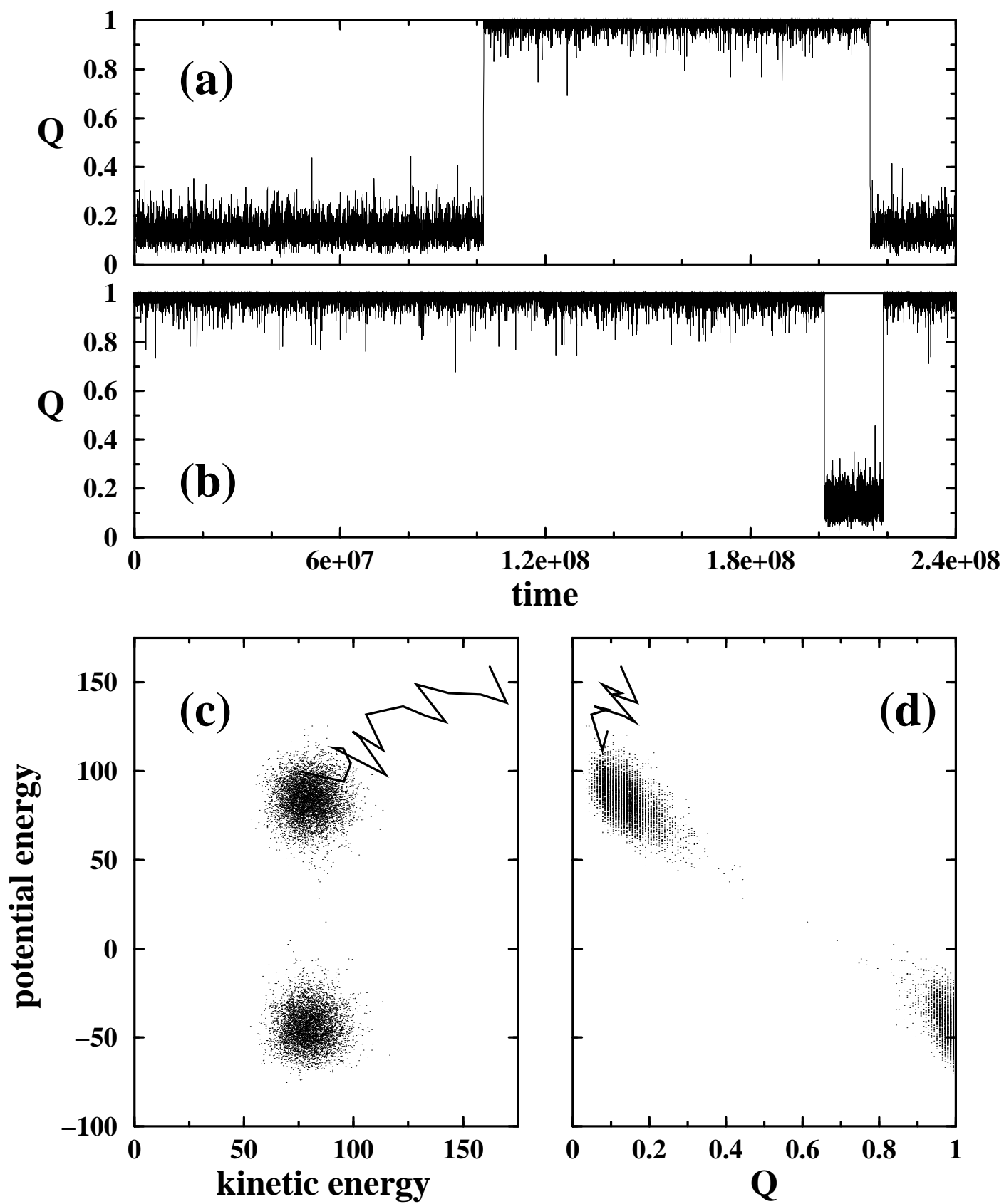


**Fig.6**

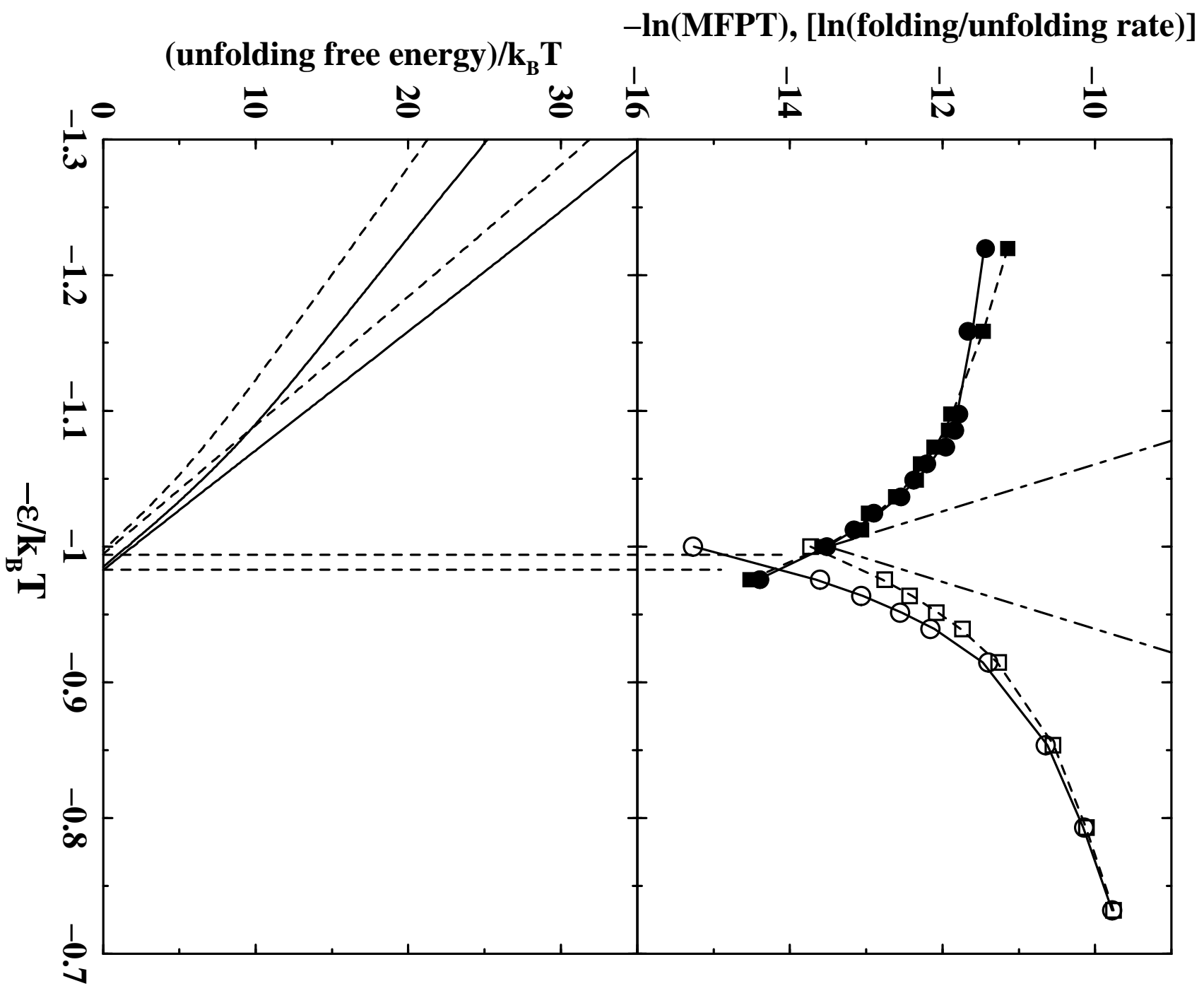


Fig.7

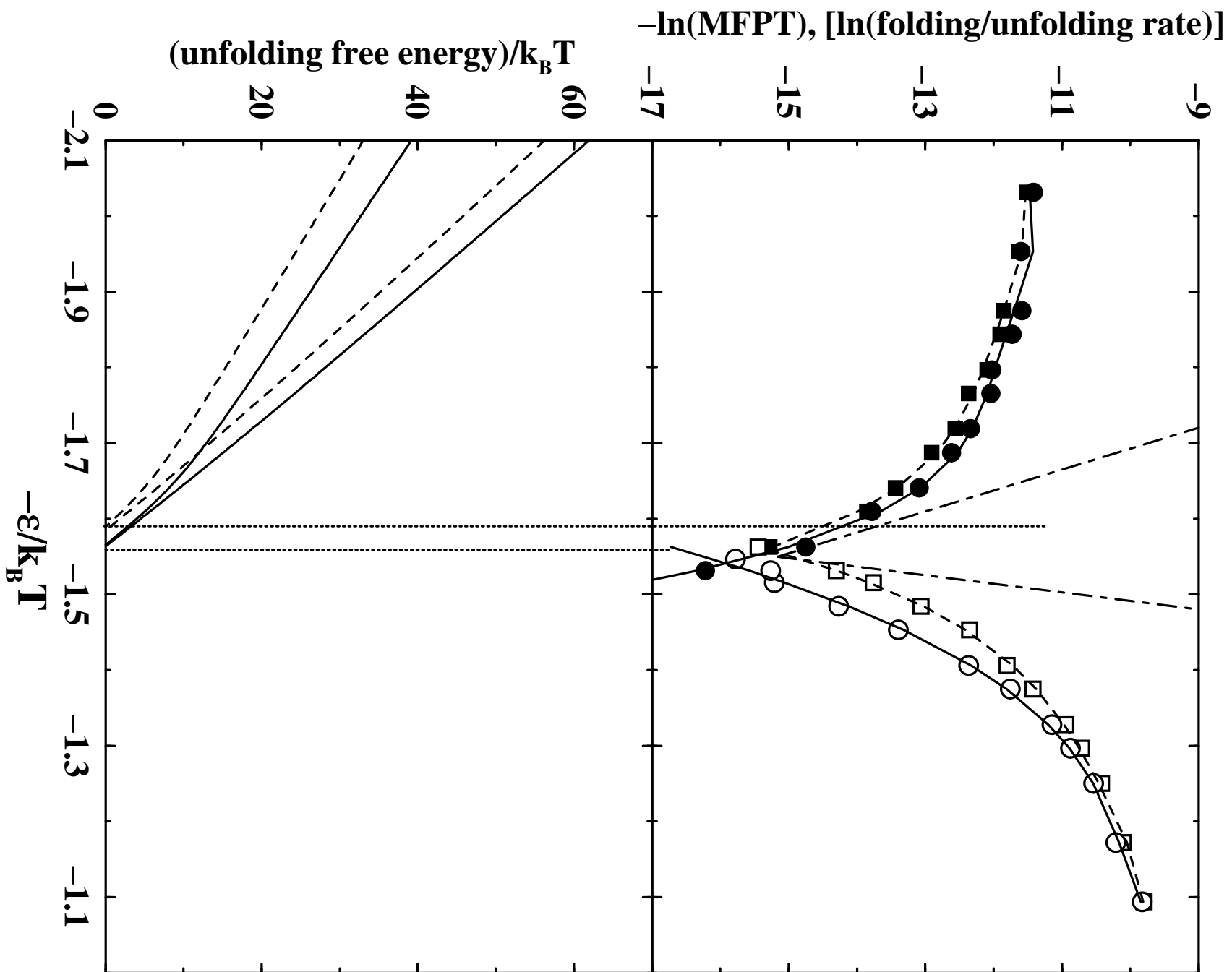


Fig.8

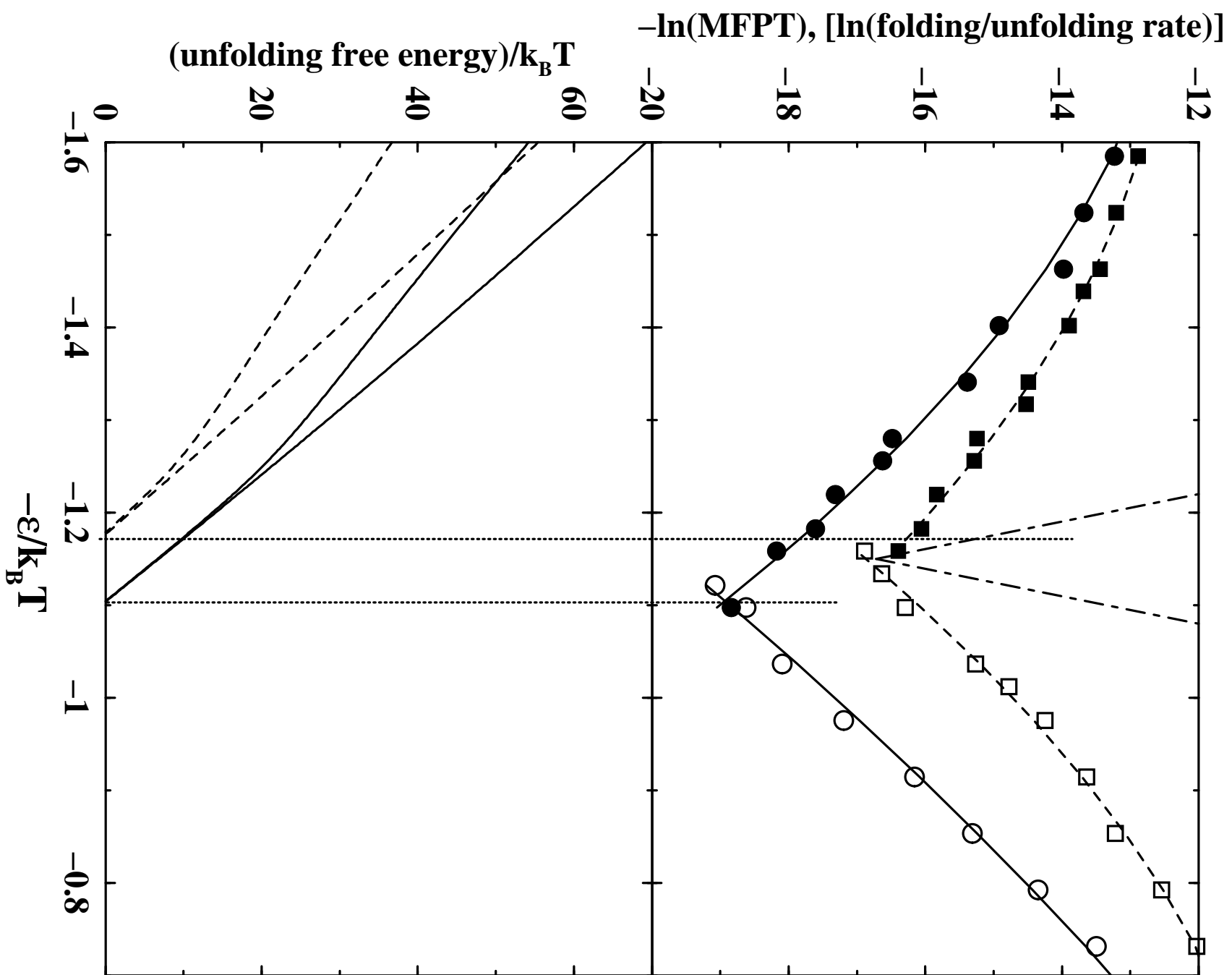


Fig.9

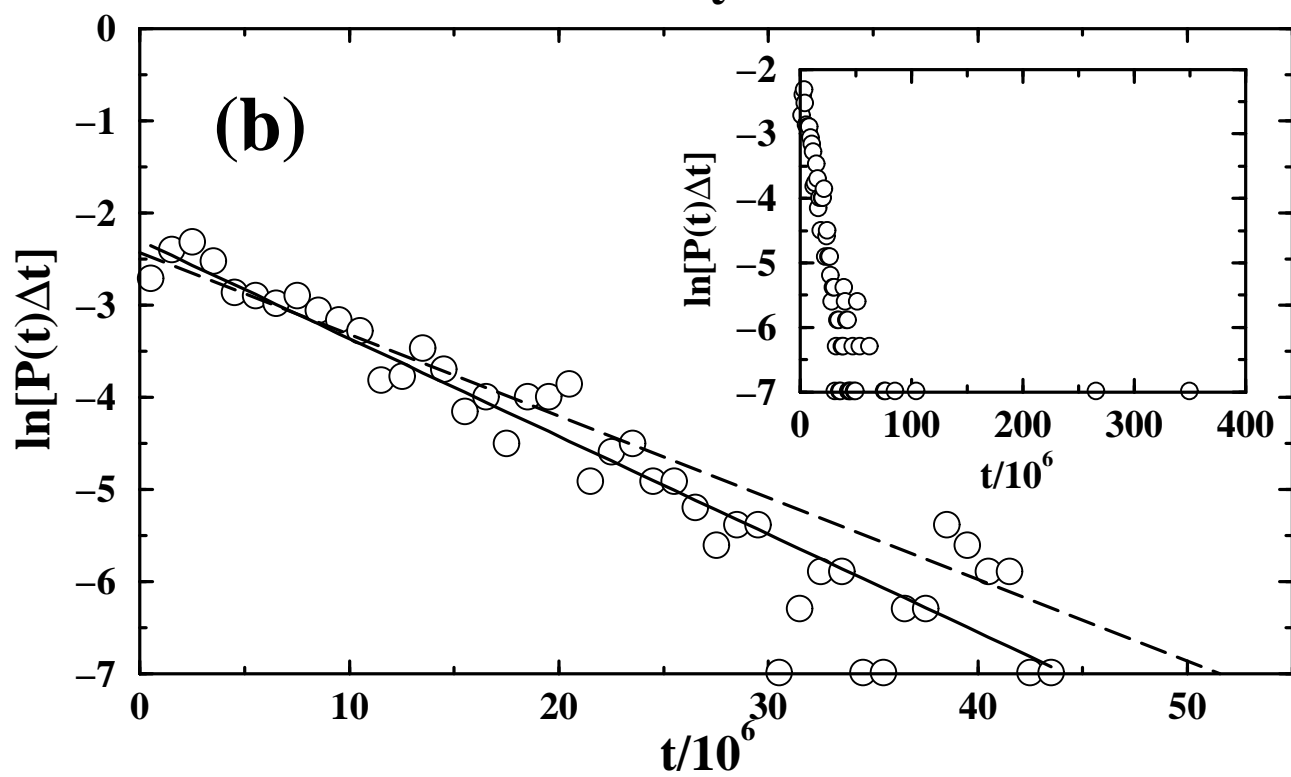
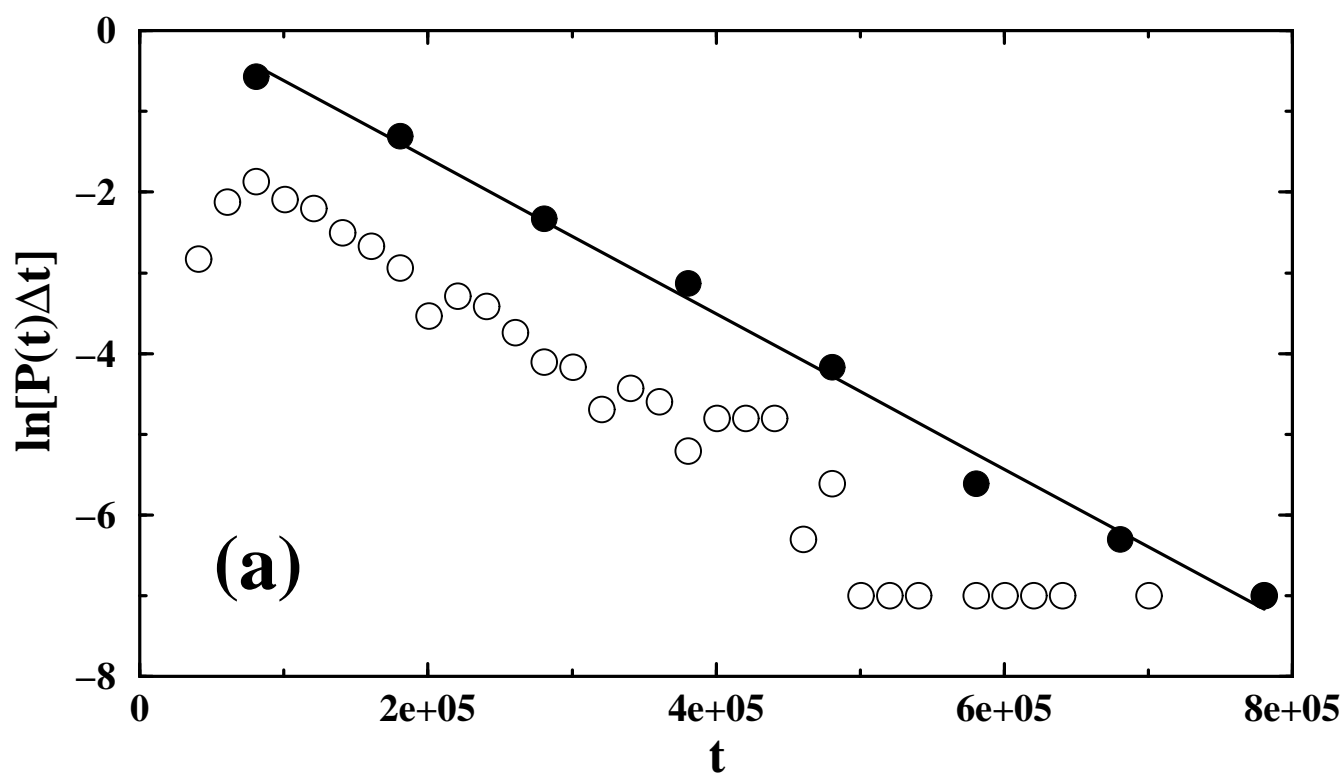


Fig.10

**Fig.11**

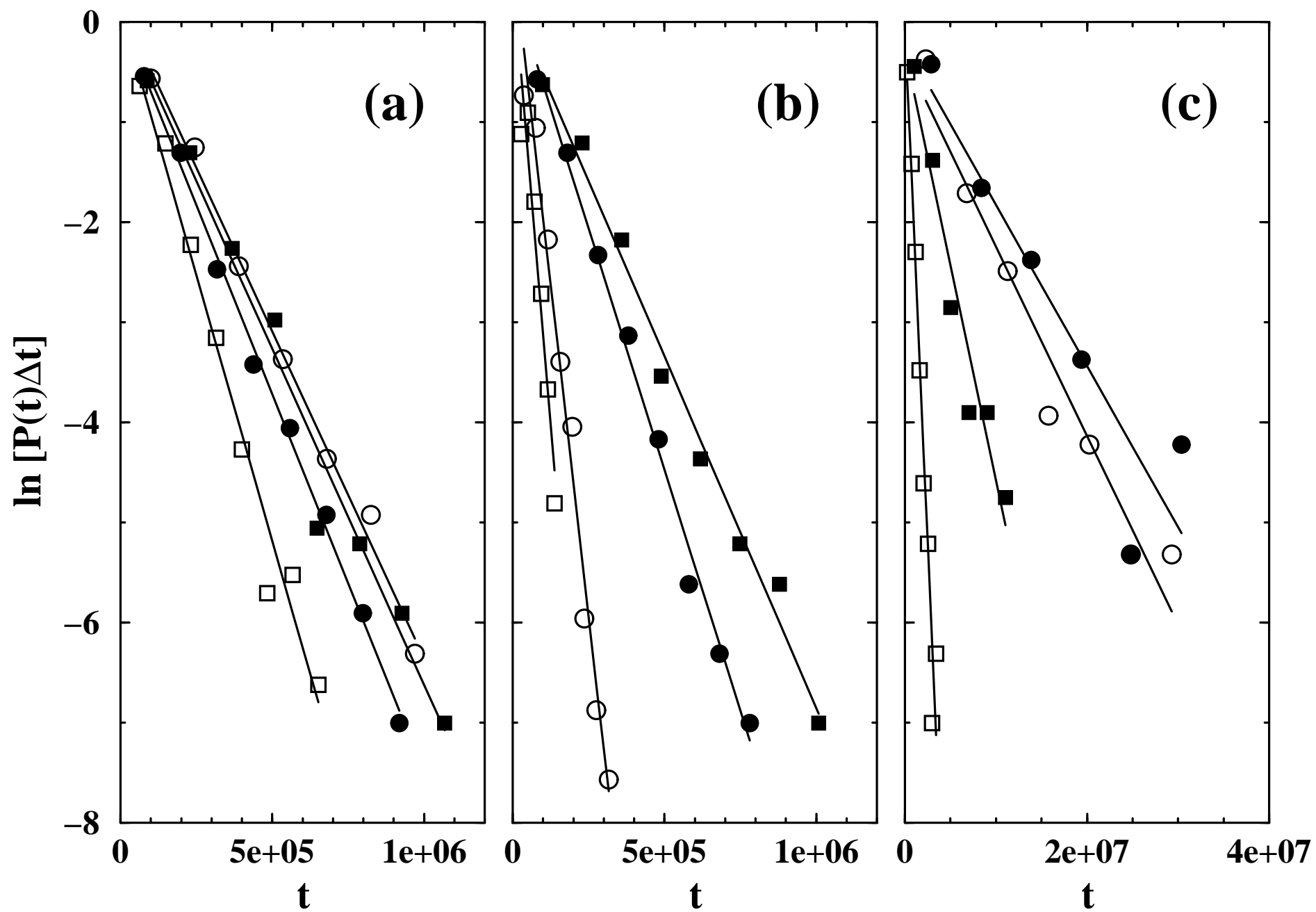


Fig.12

